Modelling land atmosphere daily exchanges of NO, NH₃, and CO₂ in a semi-arid grazed ecosystem in Senegal

Claire Delon[1], Corinne Galy-Lacaux[1], Dominique Serça[1], Erwan Personne[2], Eric Mougin[3], Marcellin Adon[1], Valérie Le Dantec[4], Benjamin Loubet[2], Rasmus Fensholt[5], Torbern Tagesson[5]

5 [1] Laboratoire d'Aérologie, Université de Toulouse, CNRS, UPS, France.
[2] INRA, EcoSys INRA-AgroParisTech, Université Paris-Saclay, Thiverval-Grignon, France.
[3] Géosciences Environnement Toulouse, Université de Toulouse, CNES, CNRS, IRD, UPS, France.
[4] Centre d'Etudes Spatiales de le BIOsphère, Université de Toulouse, CNES, CNRS, IRD, UPS, France.
[5] Department of Geosciences and Natural Resource Management, University of Copenhagen, Denmark.

10 *Correspondence to*: Claire Delon (claire.delon@aero.obs-mip.fr)

Abstract. Three different models (STEP-GENDEC-NOflux, Zhang2010 and Surfatm) are used to simulate NO, CO_2, and NH_3 fluxes at the daily scale during two years (2012-2013) in a semi-arid grazed ecosystem at Dahra (15°24'10"N, 15°25'56"W, Senegal, Sahel). Model results are evaluated against experimental results acquired during three field campaigns. At the end of the dry season, when the first rains rewet the dry soils, the model STEP-GENDEC-NOflux

15 simulate the sudden mineralization of buried litter, leading to pulses in soil respiration and NO fluxes. The contribution of wet season fluxes of NO and CO_2 to the annual mean is respectively 51% and 57%. NH_3 fluxes are simulated by two models: Surfatm and Zhang2010. During the wet season, air humidity and soil moisture increase, leading to a transition between low soil NH_3 emissions (which dominate during the dry months) to large NH_3 deposition on vegetation during wet months, Results show a great impact of the soil emission potential and a close agreement between the two models. The order of

20 magnitude of NO, NH_3 and CO_2 fluxes are correctly represented by the models, as well as the sharp transitions between seasons, specific to the Sahel region. The role of soil moisture on flux magnitude is highlighted, whereas the role of soil temperature is less obvious. The simultaneous increase of NO and CO_2 emissions and NH_3 deposition at the beginning of the wet season is attributed to the availability of mineral nitrogen in the soil and also to microbial processes which distribute the roles between respiration (CO_2 emissions), nitrification (NO emissions), volatilization and deposition (NH_3

25 emission/deposition). This objective of this study is to understand the origin of carbon and nitrogen compounds exchanges between the soil and the atmosphere, and to quantify these exchanges on a longer time scale when only few measurements have been performed.

1 Introduction

30 The Sahel is one of the largest semi-arid regions in the world and it is a transition zone between the Sahara desert in the north and the more humid Sudanese savanna in the south. In semi-arid zones, the exchanges of trace gases are strongly

influenced by hydrologic pulses defined as temporary increases in water inputs (Harms et al., 2012). In the West African Sahel (between 12°N:18°N, 15°W:10°E), soil water availability strongly affects microbial and biogeochemical processes in all ecosystem compartments (Wang et al., 2015), which in turn determines the exchange fluxes of C and N (Austin et al., 2004, Tagesson et al., 2015a, Shen et al., 2016). After a long dry period (8 to 10 months in the Sahel), the first rainfall events

5 of the wet season cause strong pulse of CO_2, N_2O, NO and NH_3 to the atmosphere (Jaeglé et al., 2004; Mc Calley & Sparks, 2008; Delon et al., 2015; Shen et al., 2016, Tagesson et al., 2016b). Anthropogenic activities have a strong impact on N and C cycling, and in large parts of the world, deposition of N compounds have several damaging impacts on ecosystem functions, such as changes in species biodiversity (Bobbink et al., 2010). The Sahel is still a protected region from this N pollution (Bobbink et al., 2010), but climate change could create an imbalance in biogeochemical cycles of nutrients

10 (Delgado-Baquerizo et al., 2013).

The emission of NO from soils leads to the formation of NO_2 and O_3 in the troposphere. Soil NO biogenic emissions from the African continent expressed in $TgN.yr^{-1}$ are considered as the largest in the world (Fowler et al., 2015) because of extended natural areas. The pulses of NO from the Sahel region at the beginning of the wet season have been shown to strongly influence the overlying NO_2 tropospheric column (Jaegle et al., 2004, Hudman et al., 2012, Zörner et al., 2016),

15 indicating the urgent need of improved understanding of the dynamics of NO pulses from this region. NH_3 emissions lead to the formation of particles in the atmosphere, such as ammonium-nitrates (NH_4NO_3), which vapour phase dissociation further produces NH_3 and HNO_3 (Fowler et al., 2015). The land-atmosphere exchange of ammonia varies in time and space depending on environmental factors such as climatic variables, soil energy balance, soil characteristics and plant phenology (Flechard et al., 2013). Emissions of these compounds involve changes in atmospheric composition (ozone and aerosol

20 production) and effects on climate (through greenhouse gas impacts).

The N exchange fluxes are also influenced by the soil N content, and the main inputs of N compounds into the soil in semi-arid uncultivated regions are biological nitrogen fixation (BNF), decomposition of organic matter (OM), and atmospheric wet and dry deposition (Perroni-Ventura et al., 2010). Soil N losses to the atmosphere involve N_2O, NH_3 and NO gaseous emissions, whereas within the soil, N can be lost via erosion, leaching and denitrification. NO emissions to the atmosphere

25 are mainly the result of nitrification processes, which is the oxidation of NH_4^+ to nitrates (NO_3^-) via nitrites NO_2^- through microbial processes (Pilegaard et al., 2013; Conrad, 1996). In remote areas, where anthropogenic emissions (such as industrial or traffic pollution) do not happen, NH_3 bidirectional exchanges are regulated through diverse processes: NH_3 is emitted by livestock excreta, by soil and litter, regulated by the availability of NH_4^+ and NH_3 in the aqueous phase (NHx), by the rate of mineralization of NH_4^+, and by the availability of water which allows NHx to be dissolved, to be taken up by

30 organisms and to be released through decomposition (Schlesinger et al., 1991, Sutton et al., 2013). Additionally NH_3 can be dry and wet deposited on soil and litter (Laouali et al., 2012; Vet et al., 2014), on leaf cuticles and stomata, and regulated by chemical interactions within the canopy air space (Loubet et al., 2012). The N cycle is closely linked to the C cycle, and it has been suggested that C-N interactions may regulate N availability in the soil (Perroni-Ventura et al., 2010). The link between N and C cycles in the soil, and their effect on OM decomposition, affect the emissions of C and N compounds to the

atmosphere. These cycles are interlinked by respiration and decomposition processes in the soil, and the balance between C and N is controlled by biological activity, mainly driven by water availability in drylands (Delgado-Baquerizo et al., 2013). Indeed, the decomposition of soil OM (and its efficiency) regulates the amount of CO_2 that is released to the atmosphere (Elberling et al., 2003).

5   Biogeochemical regional models have been applied for N compound emissions mostly in temperate regions (Butterbach-Bahl et al., 2001, Butterbach-Bahl et al., 2009), where the spatial and temporal resolution of data is well characterized. Global approaches have also been developed, with simplified description of processes and with coarse spatial resolution (Yienger & Levy, 1995; Potter et al., 1996; Yan et al., 2005; Hudman et al., 2012). Considering the weak amount of experimental data in semi-arid regions about trace gas exchanges and their driving parameters, one dimensional modelling is

10   a complementary, essential and alternative way of studying the annual cycle dynamics and the underlying processes of emission and deposition. The specificity of the semi-arid climate needs to be precisely addressed in the models used to be able to correctly represent the pulses of emissions and the strong changes in C and N dynamics at the transition between seasons. Improving the description of processes in 1D models in tropical regions is therefore a necessary step before implementing regional modelling.

15   In this study, three main modelling objectives are focused on: 1) investigating the links between N and C cycles in the soil and consecutive daily exchanges of NO, NH_3 and CO_2 between the soil and the atmosphere, at the annual scale and specifically at the transition between seasons, 2) comparing two different formalisms for NH_3 bidirectional exchange 3) highlighting the influences of environmental parameters on these exchanges. Different one dimensional models, specifically developed or adapted for semi-arid regions, were used in the study. As a study site, representative of the semi-arid region of

20   the Western Sahel, we selected the Dahra field site located in the Ferlo region of Senegal (Tagesson et al., 2015b). The one dimensional models were applied for the years 2012 and 2013 to simulate the land-atmosphere exchange fluxes of CO_2, NO and NH_3. Model results were compared to flux measurements collected during three field campaigns in Dahra in July 2012 (7 days), July 2013 (8 days) and November 2013 (10 days), and presented in Delon et al. (2017).

2 Materials and Methods

25   ### 2.1 Field site

Measurements were performed at the Dahra field station (part of the Centre de recherché Zootechnique, CRZ), in the Sahelian region of Ferlo, Senegal (15°24'10"N, 15°25'56"W). The Dahra field site is located within the Centre de Recherche Zootechnique (CRZ) managed by the Institut Sénégalais de Recherche Agronomique (ISRA). This site is a semi-arid savanna used as a grazed rangeland. The Sahel is under the influence of the West African Monsoon (cool wet southwesterly

30   wind) and the Harmattan (hot dry northeasterly wind) depending on the season. Rainfall is concentrated in the core of the monsoon season which extends from mid-July to mid-October. At Dahra, the annual rainfall was 515mm in 2012 with an average of 356mm in 2013 and 416mm for the period 1951-2013. The annual mean air temperature at 2m height was 28.4°C

in 2012 and 28.7°C in 2013, with an average of 29°C for the period 1951-2003. The most abundant tree species are *Balanites aegyptiaca* and *Acacia tortilis*, and the herbaceous vegetation is dominated by annual C4 grasses (e.g. *Dactyloctenium aegyptium*, *Aristida adscensionis*, *Cenchrus biflorus* and *Eragrostis tremula*) (Tagesson et al., 2015a). Livestock is dominated by cows, sheep, and goats, and grazing occurs permanently all year-round (Assouma et al., 2017). This site was
5   previously described in Tagesson et al., (2015b) and Delon et al., (2017).

2.1 Field data

2.2.1 Hydro-meteorological data and sensible and latent heat fluxes

A range of hydro-meteorological variables are measured by a meteorological station at the Dahra field site (*Tagesson et al., 2015b*). The hydro-meteorological variables used in this study were rainfall (mm), air temperature (°C), relative air humidity
10   (%), wind speed (m.s^{-1}), air pressure (hPa) at 2m height, soil temperature (°C), soil moisture (%) at 0.05 m, 0.10 m and 0.30 m depth, and net radiation (W.m^{-2}). Data were sampled every 30 s and stored as 15 min averages (sum for rainfall). Data have then been 3h and daily averaged for the purpose of this study.

Land-atmosphere exchange of sensible and latent heat were measured for the years 2012 and 2013 with an eddy covariance system consisting of an open-path infrared gas analyzer (LI-7500, LI-COR Inc., Lincoln, USA) and a three-axis sonic
15   anemometer (Gill instruments, Hampshire, UK) (Tagesson et al., 2015a). The sensors were mounted 9 m above the ground and data were collected at a 20 Hz rate. The post processing was done with the EddyPro 4.2.1 software (LI-COR Biosciences, 2012) and statistics were calculated for 30 minute periods. For a thorough description of the post processing of sensible and latent heat fluxes, see supplementary material of Tagesson et al. (2015b).

2.2.2 Atmospheric NH$_3$ concentrations using passive samplers

20   Atmospheric concentrations of NH$_3$ (and other compounds such as NO$_2$, HNO$_3$, O$_3$ and SO$_2$) were measured using passive samplers on a monthly basis, in accordance with the methodology used within the INDAAF (International Network to study Deposition and Atmospheric chemistry in AFrica) program (https://indaaf.obs-mip.fr) driven by the Laboratoire d'Aerologie (LA) in Toulouse. While not being actually part of the INDAAF network, the Dahra site was equipped with the same passive sampler devices and analysis of these samplers were performed following the INDAAF protocol at LA.

25   Passive samplers were mounted under a stainless-steel holder to avoid direct impact from wind transport and splashing from precipitation. The holder was attached at a height of about 1.5m above ground. All the samplers were exposed in pairs in order to ensure the reproducibility of results. The samplers were prepared at LA in Toulouse, installed and collected after one month exposure by a local investigator, and sent back to the LA. Samplers before and after exposition were stored in a fridge (4 ∘C) to minimize possible bacterial decomposition or other chemical reactions. Samplers were then analyzed by Ion
30   Chromatography (IC) to determine ammonium and nitrate concentrations. Validation and quality control of passive samplers according to international standards (World Meteorological Organization report), as well as the sampling procedure and

chemical analysis of samples, have been widely detailed in Adon et al. (2010). Monthly mean NH_3 concentrations in ppbv are calculated for the period 2012 and 2013. The measurement accuracy of NH_3 passive samplers, evaluated through covariance with duplicates and the detection limit evaluated from field blanks were estimated respectively at 14 % and 0.7 ± 0.2 ppb (Adon et al., 2010).

2.2.3 Measurements of NO, NH$_3$ and CO$_2$ (respiration) fluxes from soil

NO, NH_3 and CO_2 fluxes were measured during 7 days in July 2012, 8 days in July 2013 and 10 days in November 2013; these periods will hereafter be called J12, J13 and N13 respectively. The samples were taken at three different locations along a 500m transect following a weak dune slope (top, middle and bottom) with one location per day. Each location was then sampled every 3 days, approximately from 8 AM to 7 PM for soil fluxes, and 24 hours a day for NO and NH_3 concentrations. Between 15 and 20 fluxes were measured each day during the three campaigns.

NO and NH_3 fluxes were measured with a manual closed dynamic Teflon chamber (non-steady-state through-flow chamber, Pumpanen et al. 2004) with dimensions of 200 mm width x 400 mm length x 200 mm height. During the J12 campaign, the chamber was connected to a Thermoscientific 17C analyzer, whereas in J13 and N13, it was connected to a Thermoscientific 17I analyzer (ThermoFischer Scientific, MA, USA). The calculation of fluxes is based on an equation detailed in Delon et al. (2017), adapted from Davidson et al. (1991). The increase rate of NO and NH_3 mixing ratios used in the flux calculation equation was estimated by a linear regression fitted to data measured during 180 to 300s for NO (120s for NH_3) following the installation of the chamber on the soil, as detailed in *Delon et al.* (2017). Close to the Teflon chamber, soil CO_2 respiration was measured with a manual closed dynamic chamber (SRC-1 from PP-systems, 150 mm height x 100 mm diameter) coupled to a non-dispersive infrared CO_2/H_2O analyzer EGM-4 (PP-Systems, Hitchin, Hertfordshire, UK). Soil CO_2 respiration was measured within 30 cm to the location of the NO and NH_3 fluxes. Measurements were performed on bare soil to ensure only roots and microbe respiration. Results of NO, NH_3 and CO_2 fluxes are presented as daily means with daily standard deviations. All the methods, calculations and results from the field campaigns are fully detailed in *Delon et al.* (2017).

2.3 Modeling biogenic NO fluxes and CO$_2$ respiration in STEP-GENDEC-NOFlux

2.3.1 The STEP-GENDEC model

STEP is an ecosystem process model for Sahelian herbaceous savannas (Mougin et al*.,* 1995; Tracol et al., 2006; Delon et al., 2015). It is coupled to GENDEC which aims at representing the interactions between litter, decomposer microorganisms, microbial dynamics, and C and N pools (Moorhead and Reynolds*,* 1991). It simulates the decomposition of the organic matter and microbial processes in the soil in arid ecosystems. Information such as the quantity of organic matter (faecal matter from livestock and herbal masses) are transferred from STEP as inputs to GENDEC (Fig. 1).

Soil temperatures are simulated from air temperature according to *Parton* (1984). This model requires daily max and min air temperature, global radiation (provided by forcing data), herbaceous aboveground biomass (provided by the model), initial soil temperature, and soil thermal diffusivity. Details of equations are given in *Delon et al.* (2015) and appendix A (Parameters in table A3, variables in table A4, equations in table A5).

5 Soil moistures are calculated following the tipping bucket approach (Manabe 1969): when the field capacity is reached, the excess water in the first layer (0-2 cm) is transferred to the second layer, between 2 and 30 cm. Two other layers are defined, between 30-100 cm and 100-300 cm. Equations related to soil moisture calculation are detailed in Appendix A (table A5) and in *Jarlan et al.* (2008). This approach, while being simple in its formulation, is especially useful in regions where detailed description of the environment is not available or unknown, and where the natural heterogeneity of the soil profile is

10 high due to the presence of diverse matter fragments (buried litter, dead roots from herbaceous mass and trees, stones, branches, tunnels dug by insects and little mammals).

The STEP model is forced daily by rain, global radiation, air temperature, wind speed and relative air humidity at 2m height. Initial parameters specific to the Dahra site are listed in table A1 and site parameters in table A2 (Appendix A).

2.3.2 Respiration and biogenic NO fluxes

15 The quantity of carbon in the soil was calculated from the total litter input (from faecal and herbal mass, where faecal matter is obtained from the number of livestock heads grazing at the site, Diawara 2015, Diawara et al., 2018). The quantity of carbon is 50 % the buried litter mass. The carbon and nitrogen exchanges between pools and all equations are detailed in Moorhead & Reynolds (1991) and will not be developed here. Carbon dynamics depends on soil temperature, soil moisture and soil nitrogen (linked to microbial dynamics). The concentration of nitrogen in the soil is derived from the quantity of

20 carbon using C/N ratios.

Biogenic NO fluxes were calculated using the coupled model STEP/GENDEC/NOFlux, as detailed in Delon et al. (2015). The NOFlux model uses an Artificial Neural Network approach to estimate the biogenic NO emission from soil to the atmosphere (Delon et al., 2007, 2015). The NO flux is calculated from and depends on parameters such as soil surface temperature and moisture, soil temperature at 30cm depth, sand percentage, N input (here given as a percentage of the

25 ammonium content in the soil), wind speed, soil pH. The input of N to the soil from the buried litter is provided by STEP, and the calculation of the ammonium content in the soil coming out from this N input is provided by GENDEC. The equations used for NO flux calculation are reported in Appendix B, taken from Delon et al. (2015).

The main structure of the model is kept identical as in the Delon et al., (2015) version, except for N uptake by plants, for which the present paper proposes a formulation, detailed in Appendix C. In brief, in the previous version of the model 2% of

30 the NH_4^+ pool of the soil was used for NO emission calculation. In the current version, the NO emitted to the atmosphere results from 1% of the NH_4^+ pool in the soil minus the N absorbed by plants. The percentage of soil NH_4^+ pool used to calculate the NO emission has been changed from 2 to 1% based on Potter et al (1996) who proposed a range between 0.5 and 2%. In the present study, the 1% value was more adapted to fit experimental values.

Soil respiration is the sum of autotrophic (root only) and heterotrophic respiration. The autotrophic respiration in STEP is calculated from growth and maintenance respirations of roots and shoots (Mougin et al., 1995), following equations reported in table A5 (Appendix A). Autotrophic respiration depends on root depth soil moisture and soil temperature (2-30cm) and root biomass, which dynamics is simulated by STEP. The heterotrophic respiration is calculated in GENDEC from the

5 growth and death of soil microbes in the soil depending on the available litter C (given by STEP). Microbial respiration ρ is calculated as in equation 1.

$$\rho = (1 - \epsilon)\, Ca \qquad\qquad\qquad (1)$$

Microbial growth is $\gamma = \epsilon.Ca$. Where ϵ is the assimilation efficiency and Ca is total C available, *i.e.*, total C losses from four different litter inputs, i.e. buried litter, litter from trees, faecal matter and dry roots. Microbial death is driven by the death of

10 the living microbe mass, and the change in water potential during drying-wetting cycles (change between -1.5 and -0.01 MPa in the layer 2-30cm). These calculations are described in Moorhead & Reynolds (1991) and Delon et al., (2015) and are not reported in detail in this study. A schematic view of STEP-GENDEC-NOFlux is presented in Fig. 1.

2.4 Modeling NH$_3$ fluxes

The net NH$_3$ flux between the surface and the atmosphere depends on the concentration difference $\chi cp - C_{NH3}$, where C_{NH3}

15 is the ambient NH$_3$ concentration, and χcp is the concentration of the canopy compensation point. The canopy compensation point concentration is the atmospheric NH$_3$ concentration in the canopy for which the fluxes between the soil, the stomatal cavities and the air inside the canopy switch from emission to deposition, or vice versa (Farquhar et al., 1980, Wichink Kruit et al., 2007). The canopy compensation point concentration takes into account the stomatal and soil layers. The soil compensation point concentration (χ_g) has been calculated from the emission potential Γ_g, as a function of soil surface

20 temperature (T$_g$ in K) according to Wentworth et al., (2014):

$$\chi_g \text{ (ppb)} = 13\,587 \cdot \Gamma_g \cdot e^{-(10\,396K\,/\,Tg)} \times 10^9, \qquad\qquad (2)$$

A large Γ_g indicates that the soil has a high propensity to emit NH$_3$, considering that the potential emission of NH$_3$ depends on the availability of ammonium in the soil and on the pH ($\Gamma_g = [NH_4^+]/[H^+]$, values measured in the field and available in Delon et al., (2017)).

25 Two different models designed to simulate land atmosphere NH$_3$ bidirectional exchange are used in this study, and described below.

2.4.1 Inferential method (Zhang et al., 2010)

An inferential method was used to calculate the bi-directional exchange of NH$_3$. The overall flux F$_{NH3}$ is calculated as:

$$F_{NH3} = (\chi_{cp} - C_{NH3}) \times V_d \qquad\qquad \text{(equation 3)}$$

30 with Vd = 1/(R$_a$+R$_b$+R$_c$)

where Vd is the deposition velocity, determined by using the big-leaf dry deposition model of Zhang et al. (2003). R_a and R_b are the aerodynamic and quasi-laminar resistances respectively, R_c is the total resistance to deposition resulting from component terms such as stomatal, mesophyll, non-stomatal/external/cuticular and soil resistances (Flechard et al., 2013 and references therein). C_{NH3} is determined at the monthly scale from passive sampler measurements. The χ_{cp} term is calculated

5   following the two-layer Zhang et al. (2010) model (hereafter referred to as Zhang2010). This model gives access to an extensive literature review on compensation point concentrations and emission potential values classified for 26 different Land Use Classes (LUC). Compensation point concentrations are calculated in the model and vary with canopy type, nitrogen content, and meteorological conditions. This model was adapted by Adon et al. (2013) for the specificity of semi-arid ecosystems such as Leaf Area Index (LAI) or type of vegetation, assuming a ground emission potential of 400 (unitless)

10   (considered as a low end value for non fertilized ecosystems according to Massad et al., (2010) and based on Delon et al. (2017) experimental results) and a stomatal emission potential of 100 (unitless) (based on Massad et al. (2010) for grass, and on the study of Adon et al. (2013) for similar ecosystems as the one found in Dahra). Considering the bidirectional nature of NH_3 exchange, emission occurs if the canopy compensation point concentration is superior to the ambient concentration (Nemitz et al., 2001). Emission fluxes are noted as positive. Meteorological forcing required for the simulation are 3h-

15   averaged wind speed, net radiation, pressure, relative humidity, air temperature at 2m height, surface temperature at 5cm depth, and rainfall. The equations used in this model are extensively described in Zhang et al. (2003, 2010), and will not be detailed here.

2.4.2 The Surfatm model

The Surfatce-Atmosphere (Surfatm) model combines an energy budget model (following Choudhury and Monteith, (1988))

20   and a pollutant exchange model (following Nemitz et al., (2001)), which allows distinction between the soil and the plant exchange processes. The scheme is based on the traditional resistance analogy describing the bi-directional transport of NH_3 governed by a set of resistances controlled by the atmosphere, R_a (s m^{-1}), the quasi-laminar boundary layer, R_b (s m^{-1}), and the canopy, R_c (s m^{-1}) respectively (Hansen et al., 2017 and references therein). Surfatm includes a diffusive resistance term from the topsoil layer to the soil surface. Surfatm represents a comprehensive approach to study pollutant exchanges and

25   their link with plant and soil functioning The NH_3 exchange is directly coupled to the energy budget, which determines the leaf and surface temperatures, the humidity of the canopy, and the resistances in the layers above the soil and in the soil itself. This model has been comprehensively described in Personne et al. (2009) and more recently in Hanson et al (2017).

The model is forced every 3h by net radiation, deep soil temperature (30 cm), air temperature, relative humidity, wind speed, rainfall, atmospheric NH_3 concentration (with monthly values from passive samplers measurements repeated every 3 hours).

30   Forcing also includes constant values of roughness length Z_0, Leaf Area Index (LAI), displacement height D, canopy height Z_h, measurement height Z_{ref}, stomatal emission potential, and ground emission potential. The ground emission potential has been set to 400 (unitless), and the stomatal emission potential has been set to 100 (unitless) as in the simulation based on Zhang2010, except during field campaign periods, where the ground emission potential has been derived from experimental

values (700 in J12 and J13 and 2000 in N13). Constant input parameters were adapted to semi-arid conditions to get the best fit between measured and simulated fluxes, and their values are listed in Table 1.

The main difference between Surfatm and Zhang2010 is the presence of a SVAT (Surface Vegetation Atmosphere Transfer) model in Surfatm (Personne et al., 2009), allowing for energy budget consideration and accurate restitution of surface temperature and moisture.

2.5 Statistic analysis

Modeling and experimental results (trace gas fluxes and environmental parameters) have been analyzed on the basis of their correlation (R^2) with an indication of the p-value, and with stepwise multiple regression analysis. The R software (http://www.R-project.org) was used to provide results of this linear regression analysis.

3 Results

3.1 Soil moisture, soil temperature and land atmosphere heat fluxes

Soil moisture simulated by STEP in the surface layer (Fig. 2a) is limited at 11% during the wet season. This value corresponds to the field capacity calculated by STEP. The soil moisture modelling follows the tipping bucket approach, i.e. when the field capacity is reached, the excess water is transferred to the second layer, between 2 and 30 cm. Experimental values measured at 5 and 10 cm are better represented by the model in this second layer (Fig. 2b). Linear regression gives a R^2 of 0.74 (resp. 0.81) between STEP soil moisture in the 0-2cm (resp. 2-30cm) layer and experimental soil moisture at 5 cm. R^2 is 0.77 between STEP soil moisture in the 2-30cm layer and experimental soil moisture at 10 cm The temporal dynamics given by STEP, the filling of the surface layer, the maximum and minimum values are comparable to the data. However, the drying of the layers is sharper in the model than in measurements at the end of the wet season, hence the underestimation of the model compared to measurements until December each year.

As a comparison, linear correlation between STEP H (resp. STEP LE) and EC H (resp. EC LE) gives R^2 of 0.4 (resp. 0.7), for both years of simulation (Fig. 3a and 3b). The significant correlation between Surfatm and EC latent heat fluxes indicates that the stomatal, aerodynamic and soil resistances are correctly characterized in the model, giving confidence in the further realistic parameterization of NH_3 fluxes.

Surfatm soil surface temperature is very close to measured soil surface temperature (Fig. 4a, R^2=0.70, p<0.001 in 2012-2013). Mean annual values were 35 8°C and 34.2°C respectively for surface Surfatm and measured soil surface temperatures in 2012, and 32.4°C and 33.8°C in 2013. STEP surface temperatures (0-2cm layer) presents mean values of 32.0°C in 2012, and 32.6°C in 2013. Linear regression between STEP 0-2cm layer and measured surface temperatures (Fig. 4b) gives a R^2 of 0.7 (p<0.001) for 2012-2013.

3.2 Biogenic NO fluxes from soil

In J12, average NO fluxes are 5.1 ± 2.8 ngN.m^{-2}.s^{-1} and 5.7 ± 3.1 ngN.m^{-2}.s^{-1} for modelled and measured fluxes respectively. In J13, average NO fluxes are 10.3 ± 3.3 ngN.m^{-2}.s^{-1} and 5.1 ± 2.1 ngN.m^{-2}.s^{-1} for modelled and measured fluxes respectively. In N13, average NO fluxes are 2.2 ± 0.3 ngN.m^{-2}.s^{-1} and 4.0 ± 2.2 ngN.m^{-2}.s^{-1} for modelled and measured fluxes respectively.

5   In Fig. 5, the model represents the daily fluxes for 2012 and 2013 and is compared to measurements. The model is comprised within the standard deviation of the measurements in J12 and N13 but overestimates fluxes in J13. This overestimation may be explained by the ammonia content overestimated by the model at this period, shown in Fig. 6 which reports 9 points of measured ammonia from Delon et al., (2017). This involves an overestimation of released N during the J13 wet season, and an underestimation at the end of the wet season (as N13), when the presence of standing straw may lead to N emissions in

10   addition to soil emissions, not accounted for in the model because litter is not yet buried. The slight underestimation of modelled soil moisture (Fig. 2) at the end of the wet season may also explain why modelled fluxes are lower than measured fluxes. The large spatial heterogeneity in measurements may be explained by variations in soil pH (ranging from 5.77 to 7.43, see Delon et al., (2017)) and texture (sand between 86 and 94%, clay between 4.7 and 7.9%), and by the presence of livestock and the short term history of the Dahra site, i.e. how livestock have trampled, grazed and deposited manure during

15   the different seasons and at different places. This spatial variation is evidently not represented in the 1D model, where unique soil pH and soil texture are given, as well as a unique input of organic fertilization by livestock excreta.

Modelled dry and wet season NO fluxes are respectively 2.5 ± 2.5 ngN.m^{-2}.s^{-1} and 6.2 ± 4.1 ngN.m^{-2}.s^{-1} for both 2012 and 2013, and the simulation gives a mean flux of 3.6 ± 2.9 ngN.m^{-2}.s^{-1} for the entire study period. Wet season fluxes represent 51% of the annual mean, even though lasting only 3 to 4 months. With wet season NO fluxes being more than twice higher

20   than dry season fluxes, results emphasize the influence of pulse emissions in that season This increase at the onset of the wet season over the Sahel, due to the drastic change in soil moisture, has been previously highlighted by satellite measurements of the NO_2 column, by Vinken et al. (2014), Hudman et al. (2012), Jaegle et al. (2004) and Zörner et al. (2016).

Simulated NO fluxes are significantly correlated with measured soil moisture at 5 and 10 cm depth (R^2=0.43, $p<0.001$) for both years, but not directly with soil temperature. A multiple linear regression model involving soil moisture at 5 cm depth,

25   soil temperature at 5 and 30 cm depth and wind speed to explain simulated NO fluxes leads to a R^2 of 0.43 ($p<0.001$). These parameters have been shown as important drivers of NO emissions in several previous studies, such as Homyak et al. (2016), Medinets et al. (2015), or Delon et al. (2007). Indeed, as detailed in Appendix B, NO fluxes in STEP-GENDEC-NOflux are calculated by an equation derived from an Artificial Neural Network (ANN) algorithm taking into account these 4 parameters, together with sand percentage, soil pH and N input.

30

After the pulses of NO at the beginning of the wet season (Fig. 5), emissions decrease most likely because the available soil mineral N is used by plants during the growing phase of roots and green biomass (especially in 2013), and is less available for the production of NO to be released to the atmosphere (Homyak et al., 2014, Meixner & Fenn 2004, Krul et al., 1982).

During the wet season, NO emissions to the atmosphere in the model are reduced by 18% due to plant uptake (compared to NO emissions when plant uptake is not taken into account). Indeed, N uptake by plants is enhanced when transpiration increases during the wet season (Appendix C).

3.3 Soil CO_2 respiration

5   Soil respiration includes soil heterotrophic respiration (which refers to the decomposition of dead soil organic matter -SOM- by soil microbes) and root respiration (including all respiratory processes occurring in the rhizosphere, Xu et al., (2016)). The simulated respiration of aboveground biomass is not included as in measured data.

In J13, the average measured flux is 2.6 ± 0.6 $gC.m^{-2}.d^{-1}$, and the average modelled flux is 1.9 ± 0.4 $gC.m^{-2}.d^{-1}$. The correlation between the two data sets is non significant. In N13, the average measured flux is 0.78 ± 0.11 $gC.m^{-2}.d^{-1}$, and the average

10   modelled flux is 0.18 ± 0.02 $gC.m^{-2}.d^{-1}$. The two data sets are not correlated. November fluxes are less important than July fluxes, as illustrated by both the model and the measurements (Fig. 7), and as previously shown with eddy covariance data (Tagesson et al., 2015a). Simulated respiration fluxes are in the range of measured fluxes in J13, but appear to underestimate measured fluxes in N13 (Fig. 7), likely because the model over-predicts the death rate of microbes and subsequently underestimates the CO_2 respired, whereas microbes and residues of roots respiration persist in the field despite low soil

15   moisture. A second explanation of this underestimation might be the lower soil moisture in the model than in measurements at the end of the wet season (Fig. 2).

The simulated autotrophic respiration (roots + aboveground biomass) is shown, together with the heterotrophic (microbes) respiration, to check for a possible role of aboveground biomass in comparison with measurements (Fig. 8). As expected, the heterotrophic respiration is higher than the autotrophic respiration before and after the growth of the vegetation, i.e. at the

20   beginning and end of the wet season in 2012, or during precipitation dry spells (e.g. in J13). At the end of the wet season, the late peaks of simulated heterotrophic respiration are linked to late rain events (autotrophic respiration is no more effective because vegetation is not growing anymore). Adding the autotrophic respiration to the heterotrophic respiration does not help to better fit to measured respiration in N13.

Average dry and wet season simulated soil respiration are respectively 0.3 ± 0.7 $gC.m^{-2}.d^{-1}$ and 1.0 ± 0.4 $gC.m^{-2}.d^{-1}$, while

25   annual mean is 0.5 ± 0.7 $gC.m^{-2}.d^{-1}$. This annual mean is below global estimates for grassland (2.2 $gC.m^{-2}.d^{-1}$) and deserts partially vegetated (1.0 $gC.m^{-2}.d^{-1}$, Xu et al., 2016). The wet season has the largest contribution (57%) on the annual respiration budget (with wet seasons of 114 and 81 days in 2012 and 2013 respectively).

Simulated daily respiration from microbes and roots is significantly correlated with measured soil moisture at 5 and 10 cm depth (both with $R^2=0.5$, $p<0.001$) for both years, whereas soil field measured respiration show a lower correlation ($R^2=0.4$

30   and $p=0.09$, $R^2=0.3$ and $p=0.1$ in J13 and N13 respectively) with surface soil moisture.

3.4 NH$_3$ bidirectional exchange

NH$_3$ fluxes were simulated by two different models: Surfatm (Personne et al., 2009), and Zhang2010 (Fig.9). The same ambient concentrations deduced from in situ measurements are prescribed in both models. In J12, average fluxes are 1.3±1.1 ngN.m^{-2}.s^{-1}, 2.6±2.6 ngN.m^{-2}.s^{-1}, and -9.0±0.9 ngN.m^{-2}.s^{-1}, for measured, Surfatm and Zhang2010 respectively. Simulated

5 fluxes are not significantly correlated with measured data. In J13, average fluxes are -0.1±1.1 ngN.m^{-2}.s^{-1}, -1.7±2.4 ngN.m^{-2}.s^{-1}, -7.8±2.2 ngN.m^{-2}.s^{-1}, for measured, Surfatm and Zhang2010 respectively. Surfatm and measurements fluxes are weakly correlated (R^2=0.2 p=0.2).In N13, average fluxes are 0.7±0.5 ngN.m^{-2}.s^{-1}, -0.2±1.1 ngN.m^{-2}.s^{-1}, -2.8±0.9 ngN.m^{-2}.s^{-1}, for measured, Surfatm and Zhang2010 respectively. Surfatm and measurements fluxes are weakly correlated (R^2=0.2 p=0.2), and Zhang2010 and measurements fluxes are significantly correlated (R^2=0.5; p=0.01).

10 At the annual scale, modelled NH$_3$ dry deposition flux is -0.9±3.3 ngN.m^{-2}.s^{-1} (-0.3±1.0 kgN.ha^{-1}.yr^{-1}) and -3.5±4.6 ngN.m^{-2}.s^{-1} (-1.1±1.4 kgN.ha^{-1}.yr^{-1}) in 2012, and -2.0±3.7 ngN.m^{-2}.s^{-1} (-0.6±0.3 kgN.ha^{-1}.yr^{-1}) and -2.7±3.8 ngN.m^{-2}.s^{-1} (-0.8±1.2 kgN.ha^{-1}.yr^{-1}) in 2013, in Surfatm and Zhang2010 respectively. Fig. 9 shows alternative changes between low NH$_3$ emission and low deposition. This switch occurs during the dry seasons (from mid October to end of June). Indeed, canopy compensation point and ambient concentration values are quite similar: low deposition dominates when air humidity is

15 sufficiently high, roughly above 25% (before and after the wet season), whereas low emission dominates when air humidity is low (<25%).

Dry season fluxes are on average -0.9±2.3 ngN.m^{-2}.s^{-1} and -0.2±1.6 ngN.m^{-2}.s^{-1} and wet season fluxes are -8.1±3.2 ngN.m^{-2}.s^{-1} and -4.3±4.8 ngN.m^{-2}.s^{-1} for Zhang2010 and Surfatm respectively. The net dry and wet season fluxes are in a similar range as NH$_3$ fluxes calculated by Adon et al. (2013) using Zhang2010 at comparable Sahelian sites in Mali and Niger. NH$_3$ fluxes

20 ranged between -3.2 and 0.9 ngN.m^{-2}.s^{-1} during the dry season and between -14.6 and -6.0 ngN.m^{-2}.s^{-1} during the wet season.

4. Discussion

4.1 NH$_3$ exchanges

4.1.1 NH$_3$ deposition flux increase

25 In the months of August 2012 and 2013, there is a decrease of NH$_3$ deposition fluxes, explained by a decrease in NH$_3$ concentration (not shown here: if the concentration decreases, whereas the canopy compensation point remains stable, the flux will decrease as shown by equation 3). This decrease in NH$_3$ atmospheric concentration is explained by a strong leaching of the atmosphere in August: Dahra is a grazed savanna, and the main source of NH$_3$ emission to the atmosphere is the volatilization of livestock excreta (Delon et al., 2012); the excreta quantity and quality is at a maximum at the end of the

30 wet season, (Hiernaux et al., 1998, Hiernaux and Turner 2002, Schlecht and Hiernaux 2004), because animals are better fed.

August is the month with the maximum ammonium wet deposition, which leads to a strong leaching of the atmosphere, and explains the decrease of the NH_3 concentration (Laouali et al., 2012).

4.1.2 Role of soil moisture and soil temperature on NH_3 fluxes:

A significant correlation (p<0.01) is found between Zhang2010 and Surfatm fluxes and measured soil moisture at 5 cm depth, (0.6 and 0.3 for 2012-2013 respectively), and this correlation is higher if only the dry season is considered (0.7 and 0.5 respectively). A weak but significant correlation is found between Surfatm fluxes and soil temperature (R^2=0.2, p<0.001) for both wet seasons, whereas it is not found with Zhang2010 fluxes. An explanation may be that the NH_3 exchange in Surfatm is directly coupled with the energy balance via the surface temperature (Personne et al., 2009). A stepwise multiple linear regression analysis was performed between Zhang2010 fluxes and NH_3 ambient concentrations, air humidity, wind speed, soil surface temperature and moisture, for both years of simulation. The resulting model gives a R^2 of 0.9 (p<0.001), showing a large interdependence of the above cited parameters on NH_3 fluxes (whereas the correlation between NH_3 fluxes and each individual parameter is not significant). While the isolated soil temperature effect is not demonstrated, these complex interactions between influencing parameters suggest that the contribution of soil temperature to NH_3 fluxes, together with other environmental parameters, becomes relevant.

The same multiple linear regression model is run between Surfatm NH_3 fluxes and the above cited parameters, but with soil moisture replaced by latent heat fluxes since soil moisture in Surfatm is not available at a constant depth. R^2 is 0.6 (with p<0.001). As for Zhang2010, the nested influences of environmental parameters in Surfatm are highlighted. These interactions become more complex with the energy balance effect, but may be more accurate in representing the partition between surface and plant contributions.

4.1.3 Contribution of soil and vegetation to the net NH_3 flux in Surfatm:

Surfatm allows differentiating between the different contributions of soil and vegetation to the NH_3 fluxes (Fig. 10). The net flux above the canopy results from an emission flux from the soil and a deposition flux onto the vegetation via stomata and cuticles, especially during the wet season. Emission from stomata may also occur (Sutton et al., 1995) but is largely offset by the deposition on leaf surfaces which leads to a deposition flux onto vegetation. The deposition on cuticles is effective until the end of the wet season, whereas deposition through stomata lasts until the vegetation is completely dry, i.e. approximately 2 months after the end of the wet season (the details between stomata and cuticle deposition is not shown here). On the basis of the different averages for each contributing flux, we estimate that the soil is a net source of NH_3 during the wet season, while the vegetation is a net sink.

During the wet season, the contributions of vegetation and soil in Surfatm are -6.3±3.7 6 ngN.m^{-2}.s^{-1} and 2.0±1.9 6 ngN.m^{-2}.s^{-1} respectively for both years. Deposition on the vegetation through stomata and cuticles dominate the exchange at that time of the year, (during rain events, the cuticular resistance becomes small and cuticular deposition dominates) despite an increase of soil emission. This increase is due to an increase of the deposition velocity of NH_3 (consecutive to the humidity

13

response of the surface) and a decrease of the canopy compensation point, sensitive to the surface wetness (Wichink-Kruit et al., 2007).

During the dry season, vegetation (i.e. stomata + cuticles) and soil contributions are low (-0.9±1.7, and 0.7±0.6 ngN.m^{-2}.s^{-1} respectively, as reported in Table 2). Aboveground herbaceous dry biomass stands for a few months after the end of the wet

5   season when the soil becomes bare, and the vegetation effect negligible. At the end of wet season 2013 (Fig. 11), the soil contribution to the total flux increases significantly (2.9±0.7 ngN.m^{-2}.s^{-1} in N13) due to the increase of the ground emission potential prescribed at 2000 in Surfatm (instead of 400 for the rest of the year, to be consistent with measurements noted in Delon et al., (2017)).

4.1.4 Surfatm versus Zhang2010 NH$_3$ bidirectional models

10   The two models are based on the same two layer model approach developed in Nemitz et al. (2001). In the two models, the ground emission potential and the NH$_3$ ambient concentrations are prescribed. The comparison of modelled and measured flux values in Fig. 9 shows differences especially for results predicted by Zhang2010. This is partly because in Surfatm the ground emission potential varies with time and was specifically modified for the field campaign periods, whereas this parameter does not vary in Zhang2010. Indeed, Zhang2010 model was specifically designed to address the regional scale

15   and average temporal scales rather than hot spots or hot moments of NH$_3$ exchange. The lack of variability of the ground emission potential in Zhang2010 highlights the sensitivity of fluxes to this specific parameter for 1D modelling in semi arid soils, where the rapid turnover of N cycle and the abrupt transitions between seasons needs a high flexibility of the ground emission potential to represent the processes more closely.

In Surfatm, the temperatures (above and in the soil) are calculated through the sensible heat flux, the humidity and

20   evaporation at the soil surface are calculated through the latent heat flux. The resistances needed for the compensation point concentration and for the flux calculation are deduced from the energy budget. This allows taking simultaneously into account the role of temperature and humidity of the soil. In Zhang2010, the R_a, R_b, R_c resistances are calculated directly from the meteorological forcing, and the soil resistance is prescribed. Again, the flexibility of this parameter is more adapted than fixed values for 1D modelling.

25   However, the close correlation between both models (R^2=0.5, p<0.01) indicates a similar representation of processes in each model and emphasizes clear changes at the transition between seasons.

4.2 Effect of soil moisture and soil temperature on exchange processes

For most of the biomes the temperature strongly governs soil respiration through metabolism of plants and microbes (Lloyd and Taylor, 1994; Reichstein et al., 2005; Tagesson and Lindroth, 2007). However, in our results we found no significant

30   correlation between soil temperature and trace gas fluxes. This confirms that in the semi-arid tropical savannas, physiological activity is not limited by temperature (Archibald et al., 2009; Hanan et al., 2011; Hanan et al., 1998; Tagesson et al., 2016a; Tagesson et al., 2015a). Instead, soil moisture variability overrides temperature effects as also underlined by Jia

et al. (2006). Indeed, for low soil moisture conditions, slight changes in soil moisture may have a primordial effect, while temperature effect on microbial activities is not observable *(Liu et al.,* 2009). This may explain why soil temperature and NO, CO_2 and NH_3 fluxes are not correlated at the annual scale (dominated by dry months) as mentioned in the preceding paragraphs. Due to higher soil moisture in wet seasons ($8.1\pm2.7\%$ vs $3.2\pm1.5\%$ in dry seasons), soil temperature effect

5   becomes visible, elevated temperatures may increase microbial activity, and changes in soil temperature may have an influence on N turnover and N exchanges with the atmosphere (Bai et al., 2013).

During the dry season, substrates become less available for microorganisms, and their diffusion is affected by low soil moisture conditions (Xu et al., 2016). The microbial activity slows down gradually and stays low during the dry season (Wang et al., 2015, Borken and Matzner, 2009). De Bruin et al. (1989) have experimentally shown that drying did not kill

10   the microbial biomass during alternating wet/dry conditions at a Sahelian site. It is therefore likely that the transition from activity to dormancy or death at the end of the wet season is too abrupt in the STEP-GENDEC-NOFlux model, leading to smaller NO and CO_2 fluxes than the still rather large measured fluxes. Furthermore, the two first layers of the soil in the model dry up more sharply than what measurements indicate, and the lower modelled soil moisture has an effect on modelled fluxes.

15   During the wet season (and just before and after), the link between soil or leaf wetness (related to air humidity) and NH_3 dry deposition is straightforward, as NH_3 is highly soluble in water. Water droplets, and thin water films formed by deliquescent particles on leaf surfaces increase NH_3 dry deposition (Flechard and Fowler, 1998). This process is easily reproduced by the two models used in this study, as shown in Fig. 9 where a net NH_3 dry deposition flux is observed during the wet season.

4.3 Coupled processes of NO, CO_2 and NH_3 emissions

20   Larger CO_2 and NO fluxes were seen at the beginning of the wet season (Fig; 5 and 7), compared to the core of the wet season and to the dry season. This can be explained by the rapid response of the soil decomposers to the increase in soil moisture leading to a rapid decomposition of the litter buried during the preceding dry season (and a rapid increase in ammonia as shown in Fig. 6). A pool of enzymes remains in the soil during the dry season and ensures decomposition with the first rains even when microorganism population is not yet fully developed. Austin et al. (2004) have stated that as

25   microbial substrates decompose rapidly, microbes will be sufficiently supplied for growth and respiration, involving CO_2 emissions, and the excess N will therefore be mineralized. Indeed, the NH_4^+ dynamics controls nitrification and volatilization processes (Schlesinger and Peterjohn, 1991; McCalley et al., 2011). The NH_4^+ pool may be depleted via nitrification, involving NO emissions, and in parallel volatilized, involving concomitant NH_3 emissions. On the other hand, a major depletion of NH_4^+ pool via nitrification may favor deposition of NH_3 if NH_4^+ is no more available in the soil to be

30   volatilized.

During the dry season, as the microbial activity is reduced to its lower limit, the N retention mechanism in microbial biomass does not work anymore (N retention is linked to the mineralization of organic C caused by heterotrophic microbial activity and allows N to be available for plants), and mineral N may accumulate in the soil during this time (Perroni-Ventura et al.,

15

2010, Austin et al., 2004). Therefore, N loss should neither occur via NH_3 volatilization during that period, nor via NO emission. Furthermore, the very low soil moisture and air humidity do not stimulate NH_3 deposition on bare soil or vegetation (if present) during the dry season, knowing that NH_3 is very sensitive to ambient humidity. NH_3, NO and CO_2 fluxes are affected by the same biotic and abiotic factors, including amount of soil organic C, N quantity and availability,

5   soil oxygen content, soil texture, soil pH, soil microbial communities, hydro-meteorological conditions, amount of above and below ground biomass, species composition and land use (Xu et al., 2016, Pilegaard et al., 2013, Chen et al., 2013).

At the end of the wet season, the increase of the senescent aboveground biomass increases the quantity of litter which leads to an input of new organic matter to the soil and therefore a new pool of mineral N available for the production of NO and NH_3 to be released to the atmosphere, at a time where herbaceous species no longer would benefit from it. This process has

10   been highlighted in Delon et al. (2015) in a similar dry savanna in Mali. Furthermore, NO and NH_3 emissions are suspected to come from the litter itself, as shown in temperate forests by Gritsch et al. (2016), where NO litter emissions increase with increasing moisture.

In the STEP-GENDEC-NOFlux model respiration and soil NO fluxes were significantly correlated (R^2=0.6, p<0.001), but not directly in the measurements, due to the spatial variability of the site. The microbial activity is not efficient enough in

15   the model when the soil moisture is low, whereas in measurements, as for NO fluxes, this microbial activity seems to remain at a residual level leading to a release of both NO and CO_2 to the atmosphere *(Delon et al., 2017). A lagged relationship may somehow be displayed in measurements if measured NO fluxes are shifted by 1 day (i.e. CO_2 is in advance) in J13, then R^2=0.6 (p=0.03, R^2=0.2 if not shifted), highlighting a lag between CO_2 and NO emission processes. If the same lag is applied in model predictions, then R^2=0.6, (p<0.001), showing that soil respiration and nitrification processes (causing NO release)

20   are closely linked by microbial processes through soil microorganisms that trigger soil respiration and decomposition of soil organic matter (Xu et al., 2008, Ford et al., 2007). This one day lag however has to be considered as an open question. The exact lag duration should be studied more thoroughly, but highlights anyway the close relationship between processes of nitrification and respiration.

5 Conclusions

25   This study has shown that NH_3, NO and CO_2 exchanges between the soil and the atmosphere are driven by the same microbial processes in the soil, presupposing that moisture is sufficient to engage them, and taking into account the very specific climatic conditions of the Sahel region. Indeed, low soil and air water content are a limiting factor in semi-arid regions in N cycling between the surface and the atmosphere, whereas processes of N exchanges rates are enhanced when water content of the exchange zone (where microbial processes occur) becomes more important. The role of soil moisture

30   involved in N and C cycles is remarkable and obvious in initiating microbial and physiological processes. On the contrary, the role of soil temperature is not as obvious because its amplitude of variation is weak compared to soil moisture. Temperature effects are strongly alleviated when soil moisture is low in the dry season, and become again an influencing

parameter in the wet season for N exchange. CO_2 respiration fluxes in this study are not influenced by soil temperature variations, overridden by soil moisture variation at the seasonal and annual scale. NH_3 bidirectional fluxes, simulated by two different models, have shown a high sensitivity to the ground emission potential. The possibility of adjusting this parameter to field measurements has greatly improved the capacity of the Surfatm model to fit the observation results.

5

The understanding of underlying mechanisms, coupling biogeochemical, ecological and physico-chemical process approaches, are very important for an improved knowledge of C and N cycling in semi-arid regions. The contrasted ecosystem conditions due to drastic changes in water availability have important non linear impacts on the biogeochemical N cycle and ecosystem respiration. This affects atmospheric chemistry an climate, indicating a strong role of coupled surface

10 processes within the earth system. If changes in precipitation regimes occur due to climate change, the reduction of precipitation regimes may affect regions not considered as semi arid until now, and drive them to semi-arid climates involving exchange processes such as those described in this study. Additionally, an increase in demographic pressure leading to increases in livestock density and changes in land uses will cause changes in soil physical and chemical properties, vegetation type and management, important factors affecting N and C exchanges between natural terrestrial ecosystems and

15 the atmosphere.

Author contribution: CD, CGL and DS planned and designed the research. EP and BL developed the Surfatm model, EM, CD and VLD developed the STEP-GENDEC-NOflux model, MA provided model results with Zhang2010 model, RF and TT provided data from the Dahra meteorological station. All authors participated to the writing of the manuscript.

20

Data availability: data used in this study are not publicly available. They are available upon request from Claire Delon (Claire.delon@aero.obs-mip.fr) for modelling outputs and measurements, and in Delon et al., (2017) for measurements. Data from the meteorological station in Dahar are available upon request from Torbern Tagesson (torbern.tagesson@ign.ku.dk) and Rasmus Fensholt (rf@geo.ku.dk).

25

Code availability: Surfatm model is available on request from Erwan Personne (erwan.personne@agroparistech.fr). STEP-GENDEC-NOflux is available on request from Eric Mougin (eric.mougin@ get.omp.eu). Zhang2010 is available on request from Leiming Zhang (leiming.zhang@ec.gc.ca).

30 *Competing interests*: The authors declare that they have no conflict of interest.

5

10 **Appendix A: Details on STEP formulations**

Parameter	Symbol	Unit	Source
Rainfall	P	mm	Dahra meteorological station
Net radiation	Rn		Dahra meteorological station
Maximum air temperature Minimum air temperature	Ta_{max}, Ta_{min}	°C	Dahra meteorological station
Incident Global Radiation	Rg	MJ m^{-2}	Dahra meteorological station
Mean relative air humidity	Hr	%	Dahra meteorological station
Wind Speed	ws	m s^{-1}	Dahra meteorological station
Climatic efficiency (PAR$_i$/Rg)	ε_c	MJ MJ^{-1}	0.466 Imbernon et al (1991)

Table A1: Daily climatic data of the Dahra station used for the forcing of STEP-GENDEC-NOFlux model.

15

20

18

Parameter	Symbol	Unit	Value	Source
Latitude	lat	°	15°24'10"N,	GPS measurement
Longitude	long	°	15°25'56"W	GPS measurement
Soil depth	Sd	m	3	measurement
Number of soil layers	Ni	-	4	
Thickness of layer i	e_i	cm	2 / 28 / 70 / 200	
Sand content of layer i	Sand(i)	%	89 / 89 / 91 / 91	Delon et al. 2017
Clay content of layer i	Clay (i)	%	7.9 / 7.9 / 7.4 /5; 5	Delon et al. 2017
pH value of layer i	pH(i)	-	6.4 / 6.4 / 6.4 / 6.4	Delon et al. 2017
Initial water content of layer i	Shum(i)	mm	0.4 / 8 / 10 / 38	Field measurement
Initial soil temperature of layer i	Ts(i)	°C	23.5 / 23.9 / 28 / 30	Field measurement
Run-off(on) coefficient	C_Ruiss	-	0	Endorehic site
Soil albedo	ω_s	-	0.45	Station scale, satellite

Initial dry mass	BMs0	g m^{-2}	10	Delon et al., 2015
Initial litter mass	BMl0	g m^{-2}	30	Delon et al., 2015
C3/C4 herb proportion	C3C4	%	43/67	Field measurement
Dicotyledon. contribution	Dicot	%	43	Field measurement
Root mass proportion of layer i (2:4)	Root	%	75 / 20 / 5	Mougin et al. (1995)

Table A2: site parameters necessary for initialization of STEP-GENDEC-NOFlux model.

5

10

19

Parameter	Symbol	Unit	Value	Source
Vegetation				
Vegetation albedo	ω_v	-	0.2	Station measurement, satellite
Canopy Extinction coefficient for green vegetation	k_c	-	0.475	Mougin et al., 2014
PAR extinction coefficient	k_{fAPAR}	-	0.581	Mougin et al., 2014
Maximum conversion efficiency	ε_{max}	g DM MJ^{-1}	4 [4 - 8]	Scaling parameter
Initial aboveground green mass	BMg0	g m^{-2}	0.8 [0.1, 3]	Scaling parameter
Specific Plant Area at emergence	SLAg0	m^2 g^{-1}	0.018 [0.01 – 0.03]	Scaling parameter
Slope of the relation SLA(t)	k_{SLA}	-	0.028	Unpublished data (Mougin)
Specific Plant Area for dry mass	SLAd	m^2 g^{-1}	0.0144	Unpublished data (Mougin)
Shoot maintenance respiration cost	m_{cs}		0.015 (20°)	Breman & de Ridder, 1991
Root maintenance respiration cost	m_{cr}		0.01 (20°)	Breman & de Ridder, 1991
Shoot growth conversion efficiency	Y_G	-	0.75	McCree, 1970
Root growth conversion efficiency	Y_{Gr}	-	0.8	Bachelet et al., 1989
Green mass senescence rate	S	d^{-1}	0.00191	Mougin et al., 1995
Live root senescence rate	s_r	d^{-1}	0.00072	Nouvellon, 2000
Optimal temperature for photosynthesis	Tmax	°C	38	Penning de Vries & Djitèye, 1982
Leaf water potential for 50% stomatal closure	$\psi_{1/2}$	MPa	0.6	Rambal & Cornet, 1982
Shape parameter	N	-	5	Rambal & Cornet, 1982
Minimum stomatic resistance	r_{min}	s m^{-1}	100	Körner et al 1979

C4 Mesophyll resistance	r_m	s m^{-1}	44	Jones, 1992
C3 Mesophyll resistance	r_m	s m^{-1}	450	Jones, 1992
Plant resistance to water transfert	r_p	bar d mm^{-1}	1.03	Saugier, 1974
Parameters of the canopy height curve	a, b, c	-	-0.0000024, 0.0055, 0.047	Mougin et al., 1995
Soil				
Infiltration time constant	K(i)	cm day^{-1}	1200/ 120/ 120/ 80	Casenave & Valentin, 1989
Soil Extinction coefficient	k_e	cm^{-1}	0.125 (sand) 0.135 (clay+silt)	Van Keulen, 1975
Parameters of the soil water resistance equation	a, b	-	4140, 805	Camillo& Gurney, 1986
Parameters of the soil characteristic retention curve	ai bi	- (e-5)	3.95/5.42/6.97/9.80 2.93/2.71/2.59/2.43	Modified from Cornet, 1981
Initial soil Carbon content	Cs	gC m-2	50	Unpublished data
Initial soil N content	Ns	gN m-2	3	Unpublished data

Table A3: model parameters used to run STEP-GENDEC-NOFlux model.

5

10

15

21

Variable	Symbol	Unit
Climate		
Global radiation	Rg	MJ d^{-1}
Net radiation	Rn	MJ d^{-1}
Available energy (Rn – G)	A	MJ d^{-1}
Soil heat flux	G	MJ d^{-1}
Water budget		
Rainfall	P	mm d^{-1}
Infiltration	I	mm d^{-1}
Soil water content	W	mm
Evaporation	E	mm d^{-1}
Transpiration	Tr	mm d^{-1}
Drainage	D	mm d^{-1}
Soil water potential	$\psi_{s,i}$	MPa
Soil resistance to water-vapor transfert	r_{ss}	s m^{-1}
Canopy stomatal resistance to water vapor transfer	r_{sc}	s m^{-1}
Vegetation		
Vegetation cover fraction (total)	Vcft	m^2 m^{-2}
Vegetation cover fraction (total)	Vcfg	m^2 m^{-2}
Vegetation cover fraction (total)	Vcfd	m^2 m^{-2}
Green leaf area index	LAI$_g$	m^2 m^{-2}
Dry leaf area index	LAI$_d$	m^2 m^{-2}
Specific Leaf Area	SLA	m^{-2}kg^{-1}
Canopy height	h$_c$	m
Allocation factor	a	-
Green herbage mass	BMg	g DM m^{-2}
Dry herbage mass	BMs	g DM m^{-2}
Litter herbage mass	BMl	g DM m^{-2}

Root herbage mass	BMr	g DM m^{-2}
Gross photosynthesis	PSN	g DM m^{-2}
Shoot maintenance respiration	Rmg	g DM m^{-2}
Root maintenance respiration	Rmr	g DM m^{-2}
Shoot growth respiration	Rgm	g DM m^{-2}
Root growth respiration	Rgr	g DM m^{-2}

Table A4: model variables used to run STEP-GENDEC-NOFlux. DM=Dry Matter.

5

10

15

20

25

Biogeosciences Open Access
Discussions
EGU

Equations	Unit	Source
Temperature		
Soil temperature		Parton et al., 1984
$Ts_{max} = Ta_{max} + (Er + 0.35Ta_{max})Eb$		
$Ts_{min} = Ta_{min} + 0.006BMg -1.82$		
$Er = 24.07*(1-exp(-0.000038*Radiation)$		
$Eb = exp(-0.0048*GreenBiomass) - 0.13$		
Water budget		
Infiltration I / Run-off / Run-on	mm d^{-1}	
if P<5 I=P ;		Hiernaux, 1984
if P>5 I = P + C_Ruiss*(2*P-10)		
Water infiltration in the soil profile	mm d^{-1}	Manabe, 1969
$dW_1/dt = I – E_1 – D_1$		
$dW_i/dt = D_{i-1} – E_i – Tr_i - D_i$		
if $W_i> FC$ $D_i = (D_{i-1} – FC_i)/Ak_i$		
with $Ak_i = e_i / K_i$	d^{-1}	
Soil characteristic retention curve for layer i		
$\psi_{s,i} = a_i W_i^{-bi}$	MPa	
Soil Water Content at saturation		
$Ws,i = 0.332- Sand(i)7.251e-4 +$ $0.1276log_{10}[Clay(i)]$	m^3 m^{-3}	Saxton et al., 1986
Soil Evaporation E		
$$E=Vcfs\frac{s.A+\frac{\rho C_P D}{r_{as}}}{\lambda(s+\chi(1+\frac{r_{ss}}{r_{as}}))}$$	mm d^{-1}	Monteith, 1965
Transpiration Tr		

$Tr = Vcfg \dfrac{s.A + \dfrac{\rho C_p D}{r_{ac}}}{\lambda(s + \gamma(1 + \frac{r_{sc}}{r_{ac}}))}$	mm d^{-1}	Monteith, 1965
Soil resistance to water-vapor transfert r_{ss}		
$r_{ss} = a(W_{sat} - W_1) - b$	d m^{-1}	Camillo and Gurney, 1986
Canopy stomatal resistance		
$r_{sc} = r_{s\,min}(1 + (\dfrac{\psi}{\psi_{1/2}})^n)$	d m^{-1}	Rambal and Cornet, 1982
Carbon budget		
Vegetation Cover fraction	m^2 m^{-2}	
Vcft = 1 – exp(-k$_c$ LAI)		Mougin et al., 2014
$Vcfg = Vcft \dfrac{LAIg}{LAIt}$ $Vcfd = Vcft \dfrac{LAIs}{LAIt}$		
Leaf Area Index	m^2 m^{-2}	
LAIg = SLAg*BMg LAId = SLAd*BMd SLAg=SLAg0 exp(-k$_{SLA}$ t)		Mougin et al., 1995
Canopy height	m	
h$_c$ = aBMg^2 + bBMg + c		Mougin et al, 1995

25

Biogeosciences

Discussions

Open Access

Growth model	Mougin et al., 1995; modified
Shoots and roots	$\alpha_1, \alpha_2, \alpha_3, \alpha_4$ = parameters

$$\frac{dBMg}{dt} = \alpha_1 aPSN + \alpha_2 BMg$$

$$\frac{dBMr}{dt} = \alpha_3(1-a)PSN + \alpha_4 BMr$$

Photosynthesis

$$PSN = PAR * fAPAR * f(\Psi,T) * \varepsilon_{max}$$

$f(T) = 1-(Tmax-Tl)*c$

$f(\Psi) = f(r_{smin}, r_a, r_{sc}, r_m)$

a is derived such as :

$$\frac{BMr}{BMg} = \frac{1.2}{2 + 0.01BMg}$$

ε_i= fipar = 1–exp(-k_{PAR} LAI)	fAPAR; Mougin et al., 2014

$Q_{10}(Rm) = 2^{(T-20/10)}$

Respiration

Shoot

maintenance: Rm = m_s YG BMg with	Mc Cree, 1970
m_s= m_{cs} (2.0**(Tj/10 - 2))	
growth : Rg = (1-YG)aPSN	Thornley & Cannell, 2000

Root

maintenance: Rmr = m_r YGr BMr with

mr = m_{cr} (2.0**(Ts/10 - 2))

growth :   Rgr = (1-YGr)[(1-a)PSN

Senescence

BMs = s BMg

Table A5: Equations used in STEP

Appendix B – Equations used in NOflux for NO flux calculation from ANN parameterization.

$NOFlux = c_{15} + c_{16} \times NOfluxnorm$

$NOfluxnorm = w_{24} + w_{25}\tanh(S1) + w_{26}\tanh(S2) + w_{27}\tanh(S3)$

where NOfluxnorm is the normalized NO flux

5    $S1 = w_0 + \sum\limits_{i=1}^{7} w_i x_{j,norm}$

$S2 = w_8 + \sum\limits_{i=9}^{15} w_i x_{j,norm}$

$S3 = w_{16} + \sum\limits_{i=17}^{23} w_i x_{j,norm}$

where j is 1 to 7, and $x_{1,norm}$ to $x_{7,norm}$ correspond to the seven normalized inputs, as follows:

$j = 1$: $x_{1, norm} = c_1 + c_2 \times$ (surface soil temperature),

10    $j = 2$: $x_{2, norm} = c_3 + c_4 \times$ (surface WFPS),

$j = 3$: $x_{3, norm} = c_5 + c_6 \times$ (deep soil temperature),

$j = 4$: $x_{4, norm} = c_7 + c_8 \times$ (fertilization rate),

$j = 5$: $x_{5, norm} = c_9 + c_{10} \times$ (sand percentage),

$j = 6$: $x_{6, norm} = c_{11} + c_{12} \times$ pH,

15    $j = 7$: $x_{7, norm} = c_{13} + c_{14} \times$ (wind speed).

Weights w and normalization coefficients c are given in Table B1.

w0	0.561	w14	1.611	C1	-2.454
w1	-0.439	w15	0.134	C2	0.143
w2	-0.435	w16	-0.213	C3	-4.609
w3	0.501	w17	0.901	C4	0.116
w4	-0.785	w18	-5.188	C5	-2.717
w5	-0.283	w19	1.231	C6	0.163
w6	0.132	w20	-2.624	C7	-0.364
w7	-0.008	w21	-0.278	C8	5.577
w8	-1.621	w22	0.413	C9	-1.535
w9	0.638	w23	-0.560	C10	0.055
w10	3.885	w24	0.599	C11	-25.55
w11	-0.943	w25	-1.239	C12	3.158
w12	-0.862	w26	-1.413	C13	-1.183

w13	-2.680	w27	-1.206	C14	0.614
				C15	3.403
				C16	9.205

Table B1: weights and coefficients for ANN calculation of NO flux.

Appendix C

In STEP the seasonal dynamics of the herbaceous layer is a major component of the Sahelian vegetation, and is represented through the simulation of the following processes: water fluxes in the soil, evaporation from bare soil, transpiration of the

5   vegetation, photosynthesis, respiration, senescence, litter production, and litter decomposition at the soil surface. Faecal matter deposition and decomposition is also included from the livestock total load given as input parameter.

The N uptake by plants (absorption of mineral N by plant roots) is calculated by the product of the soil water absorption by roots, with the mineral N concentration in the soil water. In the STEP model, daily root absorption is equal to the daily transpiration which depends on climatic conditions (global radiation, air temperature, wind velocity and air relative

10   humidity), soil water potential (water content in soil layers) and hydric potential of the plant which controls its stomatal aperture (and then the transpiration). Transpiration is calculated with the Penmann-Monteith equation (*Monteith,* 1965), in which the stomatal resistance depends on the plant hydric potential, itself depending on the soil moisture and climatic conditions. For equivalent climatic conditions, a dry soil involves a high potential, a closure of stomatas and a reduction of the transpiration. On the contrary, a humid soil involves a low potential, open stomatas and a large transpiration. The plant

15   hydric potential is calculated daily with transpiration equivalent to root absorption, which itself is calculated from the difference between soil and plant potentials (*Mougin et al*., 1995).

References

Adon M., C. Galy-Lacaux, V. Yoboué, C. Delon, J.P. Lacaux, P. Castera, E. Gardrat, J. Pienaar, H. Al Ourabi, D. Laouali, B. Diop, L. Sigha-Nkamdjou, A. Akpo, J.P. Tathy, F. Lavenu, and E. Mougin: Long term measurements of sulfur dioxide,

20   nitrogen dioxide, ammonia, nitric acid and ozone in Africa using passive samplers, Atmos. Chem. Phys., 10, 7467–7487, doi:10.5194/acp-10-7467-2010, 2010

Adon M., C. Galy-Lacaux, C. Delon, V. Yoboue, F. Solmon, and A.T. Kaptue Tchuente: Dry deposition of nitrogen compounds (NO_2 , HNO_3, NH_3), sulfur dioxide and ozone in west and central African ecosystems using the inferential method, Atmos. Chem. Phys., 13, 11351–11374, doi:10.5194/acp-13-11351-2013, 2013

25   Archibald, SA; A. Kirton, M.R. van der Merwe, R.J. Scholes, C.A. Williams, N. Hanan, Drivers of inter-annual variability in Net Ecosystem Exchange in a semi-arid savanna ecosystem, South Africa. Biogesciences, 6: 251-266, 2009.

.Assouma M. H, D. Serça, F. Guerin, V. Blanfort, P. Lecomte, I. Traoré, A. Ickowicz, R.J. Manlay, M. Bernoux, and J. Vayssières Livestock induces strong spatial heterogeneity of soil CO2, N2O, CH4 emissions within a semi-arid sylvo-pastoral landscape in West Africa, , Journal of Arid Land, 10 doi: 10.1007/s40333-017-0001-y, 2017.

Austin, A. T., Yahdjian, L., Stark, J. M., Belnap, J., Porporato, A., Norton, U., Ravetta, D. A., and Schaeffer, S. M.: Water pulses and biogeochemical cycles in arid and semi-arid ecosystems, Oecologia, 141, 221–235, 2004.

Bachelet D., Hunt HW, Detling JK A, simulation model of intraseasonal carbon and nitrogen dynamics of blue grama swards as influenced by above-ground and belowground grazing, Ecological Modeling Volume: 44 Issue: 3-4 Pages: 231-252, 1989.

Bai E., S. Li, W. Xu, W. Li, W. Dai and P. Jiang, A meta-analysis of experimental warming effects on terrestrial nitrogen pools and dynamics, New Phytologist, 199: 441–451, 2013.

Bobbink, R., Hicks, K., Galloway, J., Spranger, T., Alkemade, R., Ashmore, M., Cinderby, S., Davidson, E., Dentener, F., Emmett, B., Erisman, J., Fenn, M., Nordin, A., Pardo, L., Vries, W. De, Hicks, K., Galloway, J., Bobbink, R., Davidson, E., Dentener, F., Cinderby, S., Spranger, T., Bustamante, M., Global assessment of nitrogen deposition effects on terrestrial plant diversity. Ecol. Appl. 20, 30–59. doi:10.1890/08-1140.1, 2010.

Breman, H., and de Ridder, N., Manuel sur les pâturages des pays sahéliens, DLO, Centre de Recherches Agrobiologiques, Wageningen, 1991.

Borken, W., and E. Matzner, Reappraisal of drying and wetting effects on C and N mineralization and fluxes in soils. Global Change Biology, 15:808–824, 2009.

Butterbach-Bahl, K., Stange, F., Papen, H., and Li, C (2001), Regional inventory of nitric oxide and nitrous axide emissions for forest soils of southeast Germany using the biogeochemical model PnET-N-DNDC, J. Geophys. Res. 106, 34155–34166.

Butterbach-Bahl K, M. Kahl, L. Mykhayliv, C. Werner, R. Kiese, C. Li, A European-wide inventory of soil NO emissions using the biogeochemical models DNDC/Forest-DNDC, Atmospheric Environment 43, 1392–1402, 2009.

Camillo, P. J., & Gurney, R. J., A resistance parameter for bare soil evaporation models. Soil Sciences, 141, 95 – 105, 1986.

Casenave, A. and Valentin, C., Les états de surface de la zone sahélienne: influence sur l'infiltration. Ed. de l'ORSTOM, 229 pp, 1990.

Chen W., X Zheng, Q. Chen, B. Wolf, K. Butterbach-Bahl, N. Brüggemann, S. Lin, Effects of increasing precipitation and nitrogen deposition on CH_4 and N_2O fluxes and ecosystem respiration in a degraded steppe in Inner Mongolia, China, Geoderma 192, 335–340,2013.

B.J. Choudhury, J.L. Monteith, A four-layer model for the heat budget of homogeneous land surfaces Q.J.R. Meteorol. Soc., 11, pp. 373–398, 1988.

Conrad, R, Soil microorganisms as controllers of atmospheric trace gases (H_2, CO, CH_4, OCS, N_2O, and NO), Microbiol. Rev., 60, 609–640, 1996.

De Bruin B., F. W. T. Penning de Vries, L. W. Van Broekhoven, N. Vertregt, and S. C. Van de Geijn, Net mineralization, nitrification and CO2 production in alternating moisture conditions in an unfertilized low humus sandy soil from the Sahel, Plant Soil, 113, 69–78, 1989.

Delgado-Baquerizo M., F.T. Maestre, A. Gallardo, M.A. Bowker, M.D. Wallenstein, J.L. Quero, V. Ochoa, B. Gozalo, M. García-Gomez, S. Soliveres, P. García-Palacios, M. Berdugo, E. Valencia, C. Escolar, T. Arredondo, C. Barraza-Zepeda, D. Bran, J.A. Carreira, M. Chaieb, A.A. Conceiçao, M. Derak, D.J. Eldridge, A. Escudero, C.I. Espinosa, J. Gaitán, M. Gabriel Gatica, S. Gómez-González, E. Guzman, J.R. Gutiérrez, A. Florentino, E. Hepper, R.M. Hernández, E. Huber-Sannwald, M.

5   Jankju, J. Liu, R.L. Mau, M. Miriti, J. Monerris, K. Naseri, Z. Noumi, V. Polo, A. Prina, E. Pucheta, E. Ramírez, D.A. Ramírez-Collantes, R. Romão, M. Tighe, D. Torres, C. Torres-Díaz, E.D. Ungar, J. Val, W. Wamiti, D. Wang & E. Zaady, Decoupling of soil nutrient cycles as a function of aridity in global drylands, doi:10.1038/nature12670, Nature, Vol. 502, 2013.

Delon, C., Serça, D., Boissard, C., Dupont, R., Dutot, A., Laville, de Rosnay, P., and Delmas, R., Soil NO emissions
10   modelling using artificial neural network, Tellus, 59B, 502–513, 2007.

Delon, C., Galy-Lacaux, C., Boone, A., Liousse, C., Serça, D., Adon, M., Diop, B., Akpo, A., Lavenu, F., Mougin, E., and Timouk, F, Atmospheric nitrogen budget in Sahelian dry savannas, Atmos. Chem. Phys., 10, 2691–2708, doi:10.5194/acp-10-2691-2010, 2010.

Delon, C., Galy-Lacaux, C., Adon, M., Liousse, C., Serça, D., Diop, B., and Akpo, A., Nitrogen compounds emission and
15   deposition in West African ecosystems: comparison between wet and dry savanna, Biogeosciences, 9, 385–402, doi:10.5194/bg-9-385-2012, 2012.

Delon C., E. Mougin, D. Serça, M. Grippa, P. Hiernaux, M. Diawara, C. Galy-Lacaux1, and L. Kergoat, Modelling the effect of soil moisture and organic matter degradation on biogenic NO emissions from soils in Sahel rangeland (Mali), Biogeosciences, 12, 3253–3272, 2015.

20   Delon C., C. Galy-Lacaux, D. Serça, B. Loubet, N. Camara, E. Gardrat, , I. Saneh, R. Fensholt, T. Tagesson, V. Le Dantec, B. Sambou, C. Diop, E. Mougin, Soil and vegetation-atmosphere exchange of NO, NH_3, and N_2O from field measurements in a semi-arid grazed ecosystem in Senegal, Atmospheric Environment 156, 36-51, 2017.

Diawara, M.. Impact de la variabilité climatique au nord Sahel (Gourma) sur la dynamique des ressources pastorales et leurs conséquences sur les productions animales (Ph.D. thesis), Toulouse Univ., 150 p., 2015.

25   Diawara M., 2 2 2 P. Hiernaux , E. Mougin , M. Grippa , C. Delon et H.S. Diakité, Effets de la pâture sur la dynamique de la végétation herbacée au Sahel (Gourma, Mali) : une approche par modélisation, Cahiers de l'Agriculture, 27, 15010, 2018.

Elberling B., R. Fensholt, L. Larsen, A-I. S. Petersen & I. Sandholt, Water content and land use history controlling soil CO2 respiration and carbon stock in savanna soil and groundnut fields in semi-arid Senegal, Geografisk Tidsskrift-Danish Journal of Geography, 103:2, 47-56, DOI: 10.1080/00167223.2003.10649491,2003.

30   Farquhar, G. D., Firth, P. M., Wetselaar, R., and Weir, B, On the gaseous exchange of ammonia between leaves and the environment: determination of the ammonia compensation point, Plant Physiol., 66, 710–714,1980.

Flechard C.R. and D. Fowler, Atmospheric ammonia at a moorland site. II: Long-term surface-atmosphere micrometeorological flux measurements, Q. J. R. M. S., Volume 124, Issue 547, Part A, Pages 759–791,1998.

Flechard C.R., R.-S. Massad, B. Loubet, E. Personne, D. Simpson, J. O. Bash, E. J. Cooter, E. Nemitz, and M. A. Sutton, Advances in understanding, models and parameterizations of biosphere-atmosphere ammonia exchange, Biogeosciences, 10, 5183–5225, 2013.

Ford D.J., W.R. Cookson, M.A. Adams, P.F. Grierson, Role of soil drying in nitrogen mineralization and microbial
5 community function in semi-arid grasslands of north-west Australia, Soil Biology & Biochemistry 39, 1557–1569, 2007.

Fowler D., C. E. Steadman, D. Stevenson, M. Coyle, R. M. Rees, U. M. Skiba, M. A. Sutton, J. N. Cape, A. J. Dore, M. Vieno, D. Simpson, S. Zaehle, B. D. Stocker, M. Rinaldi, M. C. Facchini, C. R. Flechard, E. Nemitz, M. Twigg, J. W. Erisman, K. Butterbach-Bahl, and J. N. Galloway, Effects of global change during the 21st century on the nitrogen cycle, Atmos. Chem. Phys., 15, 13849–13893, 2015.

10 Gritsch C., F. Egger, F. Zehetner, and S. Zechmeister-Boltenstern, The effect of temperature and moisture on trace gas emissions from deciduous and coniferous leaf litter, J. Geophys. Res. Biogeosci., 121, 1339–1351, doi:10.1002/2015JG003223, 2016.

Hanan, N., N. Boulain, C. Williams, R. Scholes, and S. Archibald, Functional convergence in ecosystem carbon exchange in adjacent savanna vegetation types of the Kruger National Park, South Africa. In: M.J. Hill and N. Hanan (Editors),
15 Ecosystem Function in Savannas. CRC Press, Boca Raton, pp. 57-76, 2011.

Hanan, N., P. Kabat, J. Dolman, and J.A.N. Elbers, Photosynthesis and carbon balance of a Sahelian fallow savanna. Global Change Biol., 4(5): 523-538, 1998.

Harms, T. K., and N. B. Grimm, Responses of trace gases to hydrologic pulses in desert floodplains, J. Geophys. Res., 117, G01035, doi:10.1029/2011JG001775, 2012.

20 Hiernaux P., Fernandez-Rivera, S., Schlecht, E., Turner, M. D., and Williams, T. O., Livestock-mediated nutrient transfers in Sahelian agro-ecosystems, edited by: Renard, G., Neef, A., Becker, K., and von Oppen, M., Soil fertility management in West African land use systems, Niamey, Niger, 4-8.03.97, Margraf Verlag, Weikersheim, Germany, 339–347, 1998.

Hiernaux, P. and Turner, M. D, The influence of farmer and pastoralism management practices on desertification processes in the Sahel, in: Global desertification: do humans cause deserts?, edited by: Reynolds, J. F. and Stafford Smith, D. M.,
25 Dahlem University Press, Berlin, 135–148, 2002.

Homyak PM, Sickman J.O., Influence of soil moisture on the seasonality of nitric oxide emissions from chaparral soils, Sierra Nevada, California, USA. Journal of Arid Environments, 103, 46-52, 2014.

Homyak P.M., M. Kamiyama, J.O. Sickman, and J. P. Schimel, Acidity and organic matter promote abiotic nitric oxide production in drying soils, Global Change Biology, doi: 10.1111/gcb.13507, 2016.

30 Hudman, R. C., Moore, N. E., Mebust, A. K., Martin, R. V., Russell, A. R., Valin, L. C., and Cohen, R. C., Steps towards a mechanistic model of global soil nitric oxide emissions: implementation and space based-constraints, Atmos. Chem. Phys., 12, 7779–7795, doi:10.5194/acp-12-7779-2012, 2012.

Jaeglé, L., Martin, R. V., Chance, K., Steinberger, L., Kurosu, T. P., Jacob, D. J., Modi, A. I., Yoboué, V., Sigha-Nkamdjou, L., and Galy-Lacaux, C., Satellite mapping of rain-induced nitric oxide emissions from soils, J. Geophys. Res., 109, D21310, doi:10.1029/2003JD004406, 2004.

Jia B., G. Zhou, Y. Wang, F. Wang, X. Wang, Effects of temperature and soil water-content on soil respiration of grazed and ungrazed Leymus chinensis steppes, Inner Mongolia, Journal of Arid Environments 67, 60–76, 2006.

Jones, H. G., Plants and Microclimate. A Quantitative Approach to Environmental Plant Physiology, 2nd ed., Cambridge University Press, Cambridge, 428 pp, 1992.

Körner, C. H., Scheel, J. A., and Bauer, H., Maximum leaf diffusive conductance in vascular plants, Photosynthetica 13(1):45-82, 1979.

Krul J.M., FWT Penning de Vries, K Traore, Les processus du bilan d'azote, in "La productivité des pâturages sahéliens", Eds Penning De Vries FWT and Traoré F, pp 226-246, Wageningen, 1982.

Laouali D., Galy-Lacaux, C., Diop, B., Delon, C., Orange, D., Lacaux, J. P., Akpo, A., Lavenu, F., Gardrat, E., and Castera, P., Long term monitoring of the chemical composition of precipitation and wet deposition fluxes over three Sahelian savannas, Atmos. Environ., 50, 314–327, 2012.

LI-COR Biosciences, EDDYPRO Eddy Covariance Software Version 4.0 User's Guide & Reference. LI-COR Inc., Lincoln, 200 pp, 2012.

Liu, K., Crowley, D., Nitrogen deposition effects on carbon storage and fungal: bacterial ratios in coastal sage scrub soils of southern California. J. Env. Qual. 38, 2267-2272, 2009.

Lloyd, J. and Taylor, J.A., On the temperature dependence of soil respiration. Funct. Ecol., 8(3): 315-323, 1994.

Loubet B., C. Decuq, E. Personne, R. S. Massad , C. Flechard, O. Fanucci, N. Mascher, J.-C. Gueudet , S. Masson, B. Durand, S. Genermont, Y. Fauvel, and P. Cellier, Investigating the stomatal, cuticular and soil ammonia fluxes over a growing tritical crop under high acidic loads Biogeosciences, 9, 1537–1552, 2012.

Manabe´, S., Climate and the Ocean circulation: 1. The atmospheric circulation and the hydrology of the earth's surface. Monthly Weather Review, 97, 739 – 774, 1969.

Massad, R.-S., Nemitz, E., and Sutton, M. A., Review and parameterisation of bi-directional ammonia exchange between vegetation and the atmosphere, Atmos. Chem. Phys., 10, 10359–10386, doi:10.5194/acp-10-10359-2010, 2010.

McCalley, C. K. and Sparks, J. P., Controls over nitric oxide and ammonia emissions from Mojave Desert soils, Oecologia, 156, 871–881, 2008.

McCree, K. J., An equation for the rate of respiration of white clover plants grown under controlled conditions, in Prediction and Measurements of Photosynthetic Productivity (I. Setlik, Ed.), Pudoc, Wageningen, pp. 221-229, 1970.

Medinets S., Skiba, U.,. Rennenberg, H., and Butterbach-Bahl, K., A review of soil NO transformation: Associated processes and possible physiological significance on organisms, Soil Biol. Biochem., 80, 92–117, 2015.

Meixner T. and M. Fenn, Biogeochemical budgets in a Mediterranean catchment with high rates of atmospheric N deposition – importance of scale and temporal asynchrony, Biogeochemistry 70: 331–356, 2004.

Monteith, J. L., Evaporation and environment in state and movement of water in living organisms (19th symposium of the society for Experimental Biology) (pp. 205–234). UK: Cambridge University Press, 1965.

Monteith J.L., M.H. Unsworth, Principles of Environmental Physics, Edward Arnold, London, p. 291, 1990.

Moorhead, D. L. and Reynolds, J. F., A general model of litter decomposition in the northern Chihuahuan desert, Ecol.
5   Modell., 56, 197–219,1991.

Mougin E., Lo Seen D., Rambal S., Gaston A., and Hiernaux P., A Regional Sahelian Grassland Model To Be Coupled with Multispectral Satellite Data. I: Model Description and Validation, Remote Sens. Environ., 52, 181–193, 1995.

Nemitz, E., Milford, C., and Sutton, M. A., A two-layer canopy compensation point model for describing bi-directional biosphere/atmosphere exchange of ammonia, Q. J. Roy. Meteor. Soc., 127, 815–833, 2001.

10   Nouvellon Y., Rambal S., Lo Seen D., Moran M.S., Lhomme J.P., Bégué A., Chehbouni A.G. , Kerr, Y., Modelling of daily fluxes of water and carbon from shortgrass steppes. Agricultural and Forest Meteorology, 100, 137–153, 2000.

Parton, W. J.: Predicting soil temperatures in a shortgrass steppe, Soil Sci., 138, 93–101, 1984.

Penning de Vries, F. W. T., and Djitèye, M. A., La productivité des pâturages sahéliens. Une étude des sols, des végétations et de l'exploitation de cette ressource naturelle, Agric. Res. Rep. 918, Pudoc, Wageningen, 525 pp, 1982.

15   Perroni-Ventura Y., C. Montãña and F. García-Oliva,, Carbon-nitrogen interactions in fertility island soil from a tropical semi-arid ecosystem, Functional Ecology, 24, 233–242, doi: 10.1111/j.1365-2435.2009.01610.x, 2010.

Personne, E., Loubet, B., Herrmann, B., Mattsson, M., Schjoerring, J. K., Nemitz, E., Sutton, M. A., and Cellier, P., Surfatm-NH_3: a model combining the surface energy balance and bi-directional exchanges of ammonia applied at the field scale, Biogeosciences, 6, 1371–1388, doi:10.5194/bg-6-1371-2009, 2009.

20   Pilegaard K., Processes regulating nitric oxide emissions from soils, Phil. Trans. R. Soc. B 2013 368, 20130126, 2013.

Potter, C. S., Matson, P. A., Vitousek, P. M., and Davidson, E. A., Process modelin of controls on nitrogen trace gas emissions from soils worldwide, J. Geophys. Res., 101, 1361–1377, 1996

Pumpanen J., P. Kolari, H. Ilvesniemi, K. Minkkinen, T. Vesala, S. Niinistö, A. Lohila, T. Larmola, M. Morero, M. Pihlatie, I. Janssens, J. Curiel Yuste, J.M. Grünzweig, S. Reth, J.-A. Subke, K. Savage, W. Kutsch G. Østreng, W. Ziegler, P.
25   Anthoni, A. Lindroth, P. Hari,, Comparison of different chamber techniques for measuring soil CO2 efflux, Agricultural and Forest Meteorology 123, 159–176, 2004

Rambal, S., and Cornet, A., Simulation de l'utilisation de l'eau et de la production végétale d'une phytocénose sahélienne du Sénégal, Acta Oecologica Oecol. Plant 3(17),4: 381-397, 1982.

Reichstein M., ,E. Falge, D. Baldocchi, D. Papale, M. Aubinet, P. Berbigier, C. Bernhofer, N. Buchmann, T. Gilmanov, A.
30   Granier, T. Grunwald, K. Havrankova, ,H. Ilvesniemi, D. Janous, A. Knohl, T. Laurila, A. Lohila, D. Loustau, G. Matteucci, T. Meyers, F. Miglietta, J.M. Ourcival, J. Pumpanen, S. Rambal, E. Rotenberg, M. Sanz, J. Tenhunen, G. Seufert, F. Vaccari, T. Vesala, D. Yakir and R. Valentini, On the separation of net ecosystem exchange into assimilation and ecosystem respiration: review and improved algorithm. Global Change Biol., 11(9): 1424-1439, 2005.

Saugier, B., Transport de CO2 et de vapeur d'eau à l'interface végétation-atmosphére. Thèse Docteur d'Etat, Université des Sciences et Techniques du Languedoc, Montpellier, 156 pp, 1974.

Saxton KE, Rawls WJ, Romberger JS, Papendick RI, Estimating generalized soil-water characteristics from texture, Soil Science Society Of America Journal, Volume 50, Issue 4, pp 1031-1036, 1986.

5   Schlecht, E. and Hiernaux, P., Beyond adding up inputs andputs: process assessment and upscaling in modelling nutrient flows, Nutr. Cy. Agroecosys., 70, 303–319, 2004.

Schlesinger W.H., and W.T. Peterjoh, Processes controlling ammonia volatilization from Chihuahuan desert soils, Soil Biol. Biochem. Vol. 23, No. 1, 1991.

Shen W., G. D. Jenerette, D. Hui, and R.L. Scott, Precipitation legacy effects on dryland ecosystem carbon fluxes: direction,

10   magnitude and biogeochemical carryovers, Biogeosciences, 13, 425–439, 2016.

Sutton, M.A., Schjørring, J.K., Wyers, G.P., Plant atmosphere exchange of ammonia. Phil. Trans. R. Soc. London A351 (1656), 261-276, 1995.

Sutton M.A., S. Reis, S.N. Riddick, U. Dragosits, E. Nemitz, M.R. Theobald, Y. Sim Tang, C.F. Braban, M. Vieno, A.J. Dore, R.F. Mitchell, S. Wanless, F. Daunt, D. Fowler, T.D. Blackall, C. Milford, C.R. Flechard, B. Loubet, R. Massad, P.

15   Cellier, E. Personne, P.F. Coheur, L. Clarisse, M. Van Damme, Y. Ngadi, C. Clerbaux, C. Ambelas Skjøth, C. Geels, O. Hertel, R.J. Wichink Kruit, R.W. Pinder, J.O. Bash, J.T. Walker, D. Simpson, L. ́Horváth, T.H. Misselbrook, A. Bleeker, F. Dentener and W. de Vries, Towards a climate-dependent paradigm of ammonia emission and deposition, Phil Trans R Soc B 368: 20130166. http://dx.doi.org/10.1098/rstb.2013.0166, 2013.

Tagesson, T. and Lindroth, A., High soil carbon efflux rates in several ecosystems in southern Sweden, Boreal Environ.

20   Res., 12: 65–80, 2007

Tagesson, T., R. Fensholt, F. Cropley, I. Guiro, S. Horion, A. Ehammer, J. Ardö, Dynamics in carbon exchange fluxes for a grazed semi-arid savanna ecosystem in West Africa. Agr. Ecosyst. Environ., 205: 15-24, 2015a.

Tagesson, T. R. Fensholt, I. Guiro, M.O. Rasmussen, S. Huber, C. Mbow, M. Garcia, S. Horion, I. Sandholt, B. Holm-Rasmussen, F.M. Göttsche, M.-E. Ridler, N. Olèn, J.L. Olsen, A. Ehammer, M. Madsen, F.S. Olesen, J. Ardö, Ecosystem

25   properties of semi-arid savanna grassland in West Africa and its relationship to environmental variability. Global Change Biol., 21(1): 250-264, 2015b

Tagesson, T., R. Fensholt, B. Cappelaere, E. Mougin, S. Horion, L. Kergoat, H. Nieto, C. Mbow, A. Ehammer, J. Demarty, J. Ardö, Spatiotemporal variability in carbon exchange fluxes across the Sahel Agric. For. Meteorol., 226–227: 108-118, 2016a

30   Tagesson T., J. Ardö, I. Guiro, F. Cropley, C. Mbow, S. Horion, A. Ehammer, E. Mougin, C. Delon, C. Galy-Lacaux & R. Fensholt, Very high CO_2 exchange fluxes at the peak of the rainy season in a West African grazed semi-arid savanna ecosystem, Geografisk Tidsskrift-Danish Journal of Geography, http://dx.doi.org/10.1080/00167223.2016.1178072, 2016b

Thornley, JHM; Cannell, MGR, Modelling the components of plant respiration: Representation and realism, Annals of Botany, vol. 85, Issue 6, 937-937, 2000.

Van Keulen, H., Simulation of water use and herbage growth in arid regions, Simulation Monographs, Pudoc, Wageningen, 176 pp, 1975.

Vinken G. C. M, K. F. Boersma, J. D. Maasakkers, M. Adon, and R. V. Martin, Worldwide biogenic soil NOx emissions inferred from OMI NO2 observations, Atmos. Chem. Phys., 14, 10363–10381, 2014

5 Wang L., S. Manzoni, S. Ravi, D. Riveros-Iregui, and K. Caylor, Dynamic interactions of ecohydrological and biogeochemical processes in water-limited systems, Ecosphere 6(8):133. http://dx.doi.org/10.1890/ES15-00122.1, 2015.

Wichink Kruit, R. J., van Pul, W. A. J., Otjes, R. P., Hofschreuder, P., Jacobs, A. F. G., and Holtslag, A. A. M, Ammonia fluxes and derived canopy compensation points over non-fertilized agricultural grassland in the Netherlands using the new gradient ammonia – high accuracy – monitor (GRAHAM), Atmos. Environ., 41, 1275–1287, 2007

10 Xu X., H. Tian, and D. Hui,, Convergence in the relationship of CO_2 and N_2O exchanges between soil and atmosphere within terrestrial ecosystems, Global Change Biology 14, 1651–1660, doi: 10.1111/j.1365-2486.2008.01595.x,. 2008.

Xu M. and H. Shang, Contribution of soil respiration to the global carbon equation, Journal of Plant Physiology 203, 16–28, 2016

Yan, X., Ohara, T., and Akimoto, H., Statistical modelling of global soil NOx emissions, Global Biogeochem. Cy., 19,
15 GB3019, doi:10.1029/2004GB002276, 2005

Yienger, J. J. and Levy II, H., Empirical model of global soil biogenic NOx emissions, J. Geophys. Res., 100, 11447–11464, 1995

Zhang, L., Brook, J. R., and Vet, R., A revised parameterization for gaseous dry deposition in air-quality models, Atmos. Chem. Phys., 3, 2067–2082, doi:10.5194/acp-3-2067-2003, 2003.

20 Zhang, L., Wright, P. L., and Asman, W. A. H., Bi-directional air surface exchange of atmospheric ammonia – A review of measurements and a development of a big-leaf model for applications in regional-scale air-quality models, J. Geophys. Res., 115, D20310, doi:10.1029/2009JD013589, 2010.

Zörner J., M. Penning de Vries, S. Beirle, H. Sihler, P.R. Veres, J. Williams, T. Wagner, Multi-satellite sensor study on precipitation-induced emission pulses of NOx from soils in semi-arid ecosystems, Atmos. Chem. Phys., 16, 9457-9487,
25 doi:10.5194/acp-16-9457-2016, 2016.

30

Tables

Description of parameters in Surfatm	Value in this study
Time step	3 h
Characteristic length of leaves	0.03 m
Total soil depth	0.92 m
Soil density	1500 kg.m^{-3}
Radiation attenuation coefficient in the canopy	0.7
Wind attenuation coefficient in the canopy	2.3
Initial soil moisture	0.09 kg(H_2O)/kg(soil)
Dry soil moisture	0.02 kg(H_2O)/kg(soil)
Field capacity	0.14 kg(H_2O)/kg(soil)
Wilting point	0.02 kg(H_2O)/kg(soil)
Thermal conductivity of wet soil layers	2.5 W.m^{-1}.K^{-1}
Thermal conductivity of dry soil layers	1.5 W.m^{-1}.K^{-1}
Depth of temperature measurements	0.3 m
Soil porosity	0.45
Soil tortuosity	2.5

Table 1 : Input parameters for the Surfatm model

5

10

15

Average flux and standard deviation ($ngN.m^{-2}.s^{-1}$)	Ftotal (net flux)	Fsoil	Fvegetation (=Fstom + Fcut)	Fstom	Fcut
Dry seasons Surfatm	-0.2±1.6	0.7±0.6	-0.9±1.7	-0.4±0.8	-0.5±1.2
Wet seasons Surfatm	-4.3±4.8	2.0±1.9	-6.3±3.7	-1.5±2.2	-4.8±2.7
2012-2013 Surfatm	-1.4±3.5	1.1±1.3	-2.5±3.5	-0.7±1.5	-1.8±2.7
Dry seasons Zhang	-0.9±2.3				
Wet seasons Zhang	-8.1±3.2				
2012-2013 Zhang	-3.1±4.2				

Table 2: Contributions of vegetation and soil to the total NH_3 flux in SurfAtm, net NH_3 flux in Zhang, wet season mean, dry season mean and annual mean,for both years of simulation.

5

10

15

Figures
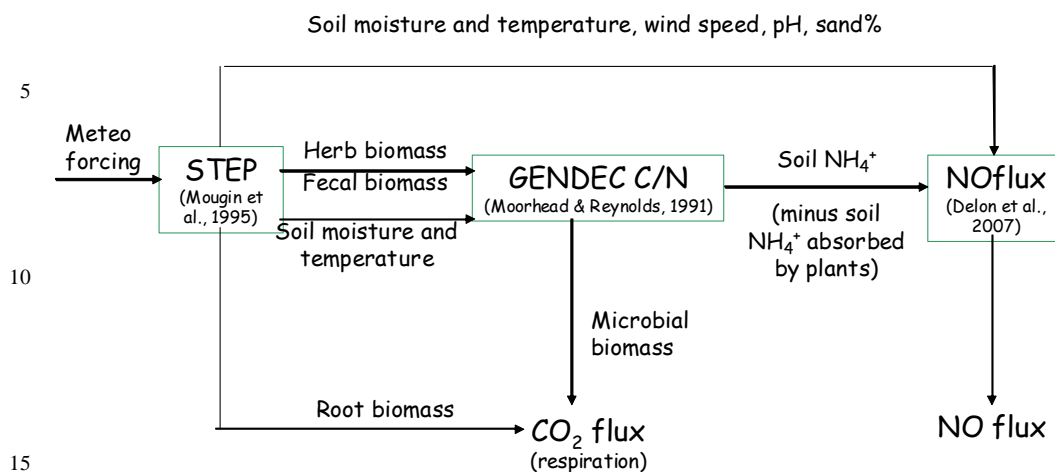
Figure 1: Schematic representation of NO and CO_2 flux modeling in STEP-GENDEC-NOFlux (adapted from Delon et al., 2015).
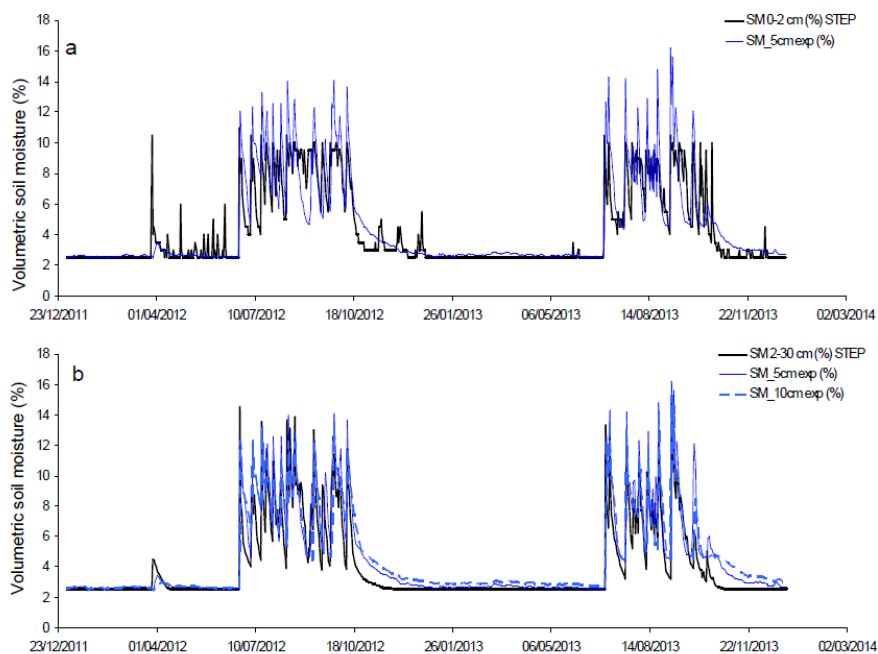
Figure 2 : a) Volumetric soil moisture simulated by STEP in the first layer (0-2cm) in black and soil moisture measured at 5cm in blue, in %, at daily scale. b) Volumetric soil moisture simulated by STEP in the second layer (2-30cm) in black, soil moisture measured at 5cm in blue solid line, measured at 10cm in blue dotted line, in %, at daily scale

5

10

15
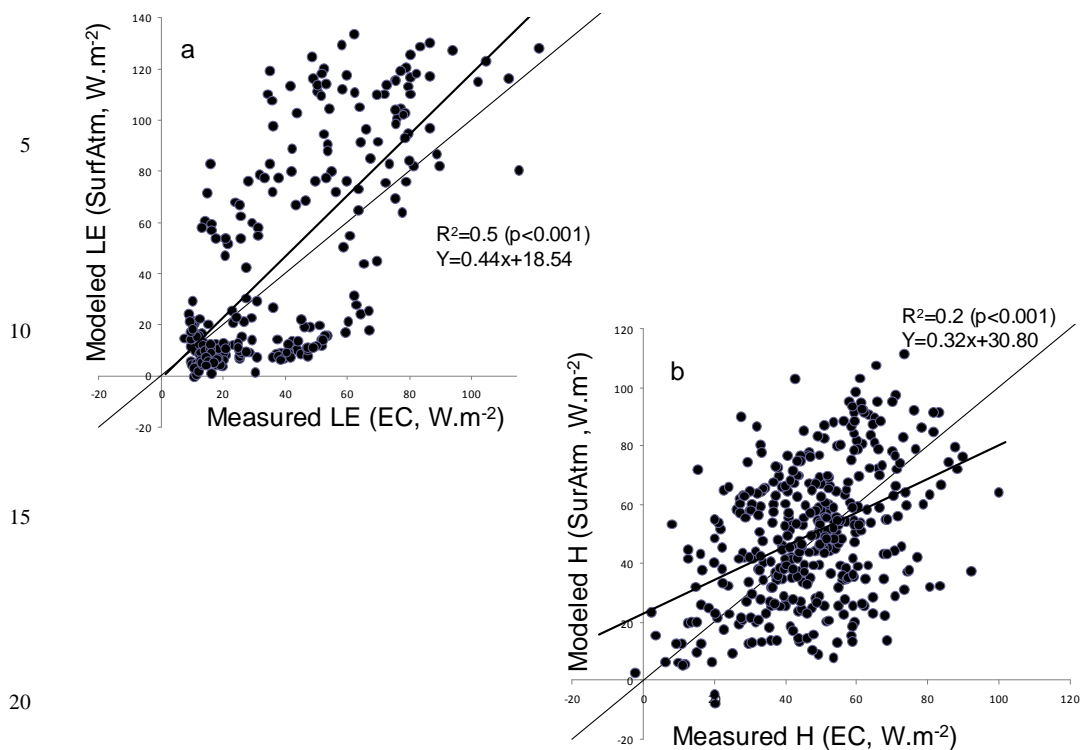
Figure 3: a) Modelled latent heat flux in SurfAtm vs measured latent heat flux, in W/m^2; b) Modelled sensible heat flux in SurfAtm vs measured sensible heat flux, in W/m^2. Thick black line is for the linear regression, thin black line is the 1:1 line. Available measured EC data are more numerous for H than for LE due to the criteria applied by the postprocessing (see supplementary material of Tagesson et al. (2015b)).

40
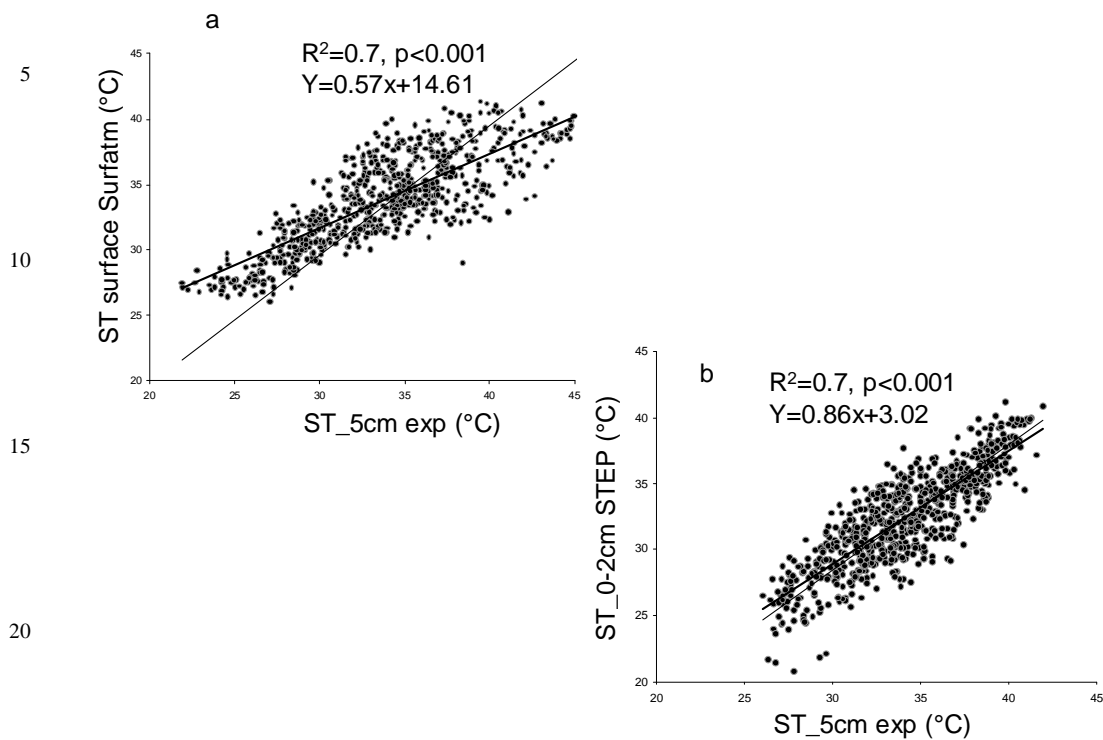
Figure 4: a) Modelled surface temperature in SurfAtm vs measured temperature at 5cm depth; b) Modelled surface temperature in STEP (0-2cm layer) vs measured temperature at 5cm depth. Thick black line is for the linear regression, thin black line is the 1:1 line
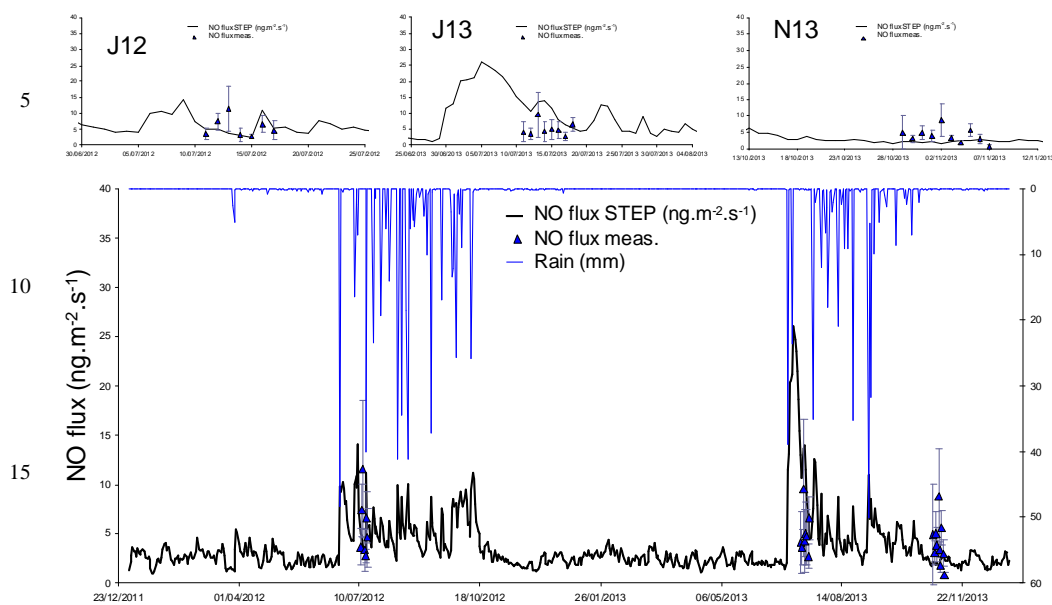
Figure 5: NO flux simulated by STEP-GENDEC-NOFlux (ngN.m⁻².s⁻¹, black line) and measured during the 3 field campaigns (blue triangles). Error bars in blue give the standard deviation at the daily scale. Rain is represented by the blue line in mm in the bottom panel. Upper panels give a focus on each field campaign.
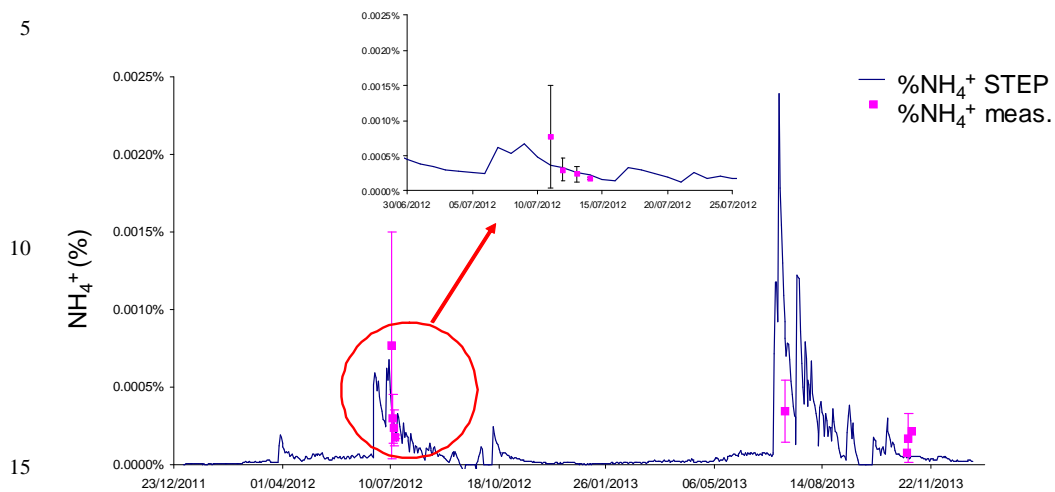
Figure 6: Ammonia simulated by STEP-GENDEC (%, blue line) and measured ammonia (pink squares) during the field campaigns. Error bars in pink give the standard deviation at the daily scale. The upper panel is a focus of J12.
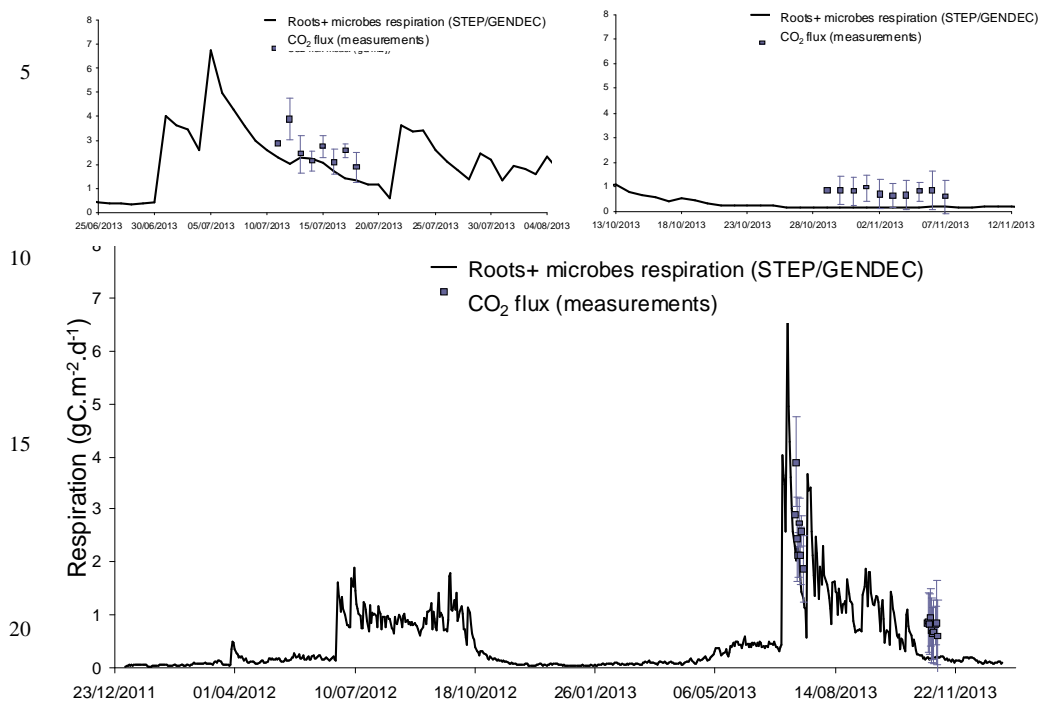
Figure 7: Roots and microbe respiration in mgC.m⁻².d⁻¹ simulated by STEP-GENDEC (black line), and soil respiration measurements (grey squares) during 2 field campaigns. Error bars in grey give the standard deviation at the daily scale
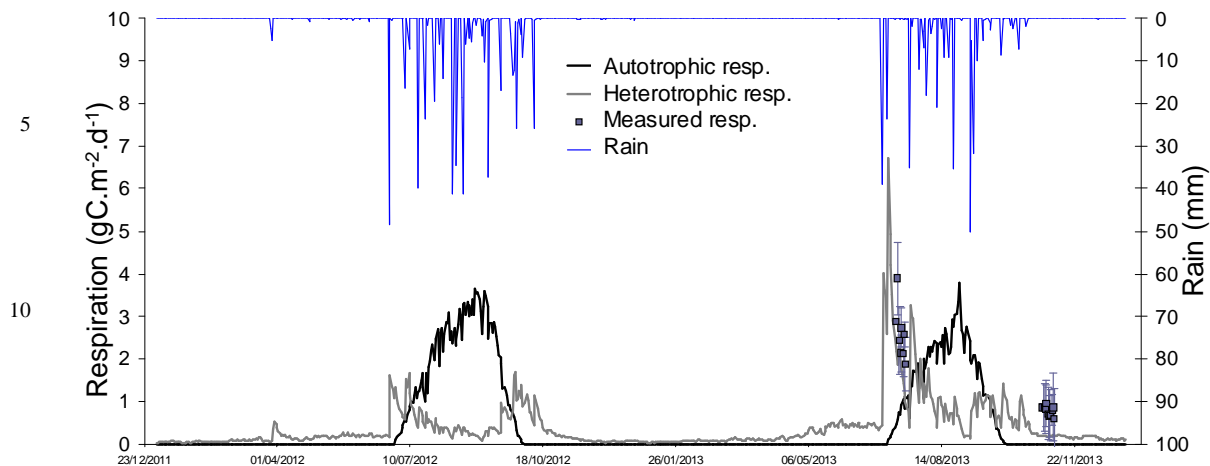
Figure 8: Autotrophic (roots + green vegetation, black line) and heterotrophic (microbes, grey line) respiration in mgC.m^{-2}.d^{-1} and rain (blue line) in mm. Measured soil respiration in grey squares, with standard deviation

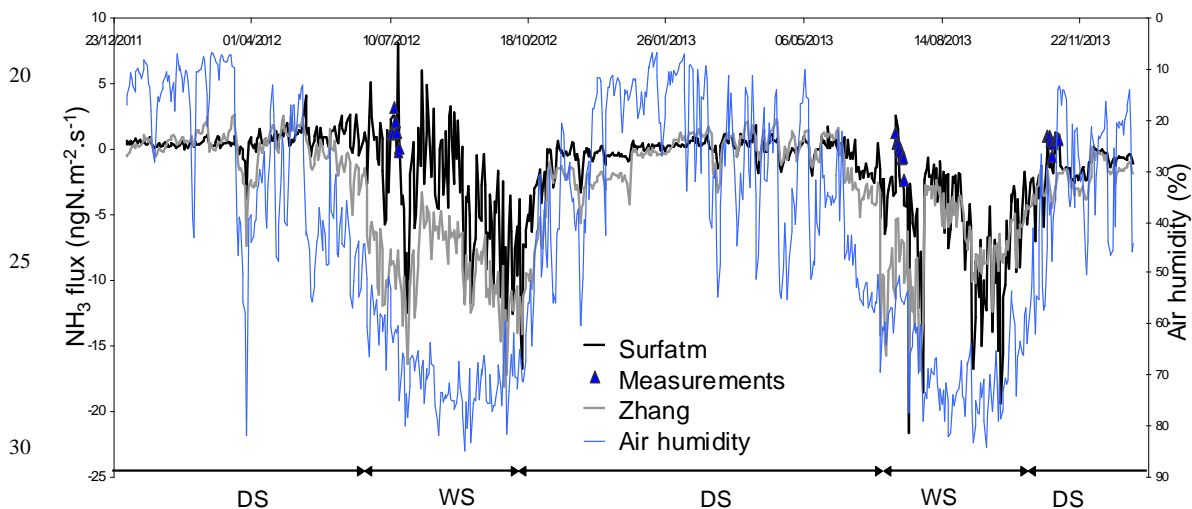**Figure 9:** NH$_3$ flux (in ngN.m^{-2}.s^{-1}) simulated by SurfAtm (black line) and Zhang et al. (2010) (grey line) and measured during 3 field campaigns (grey triangles). Error bars in grey stand for standard deviation at the daily scale. Air humidity in % (blue line). DS = Dry Season; WS = West Season
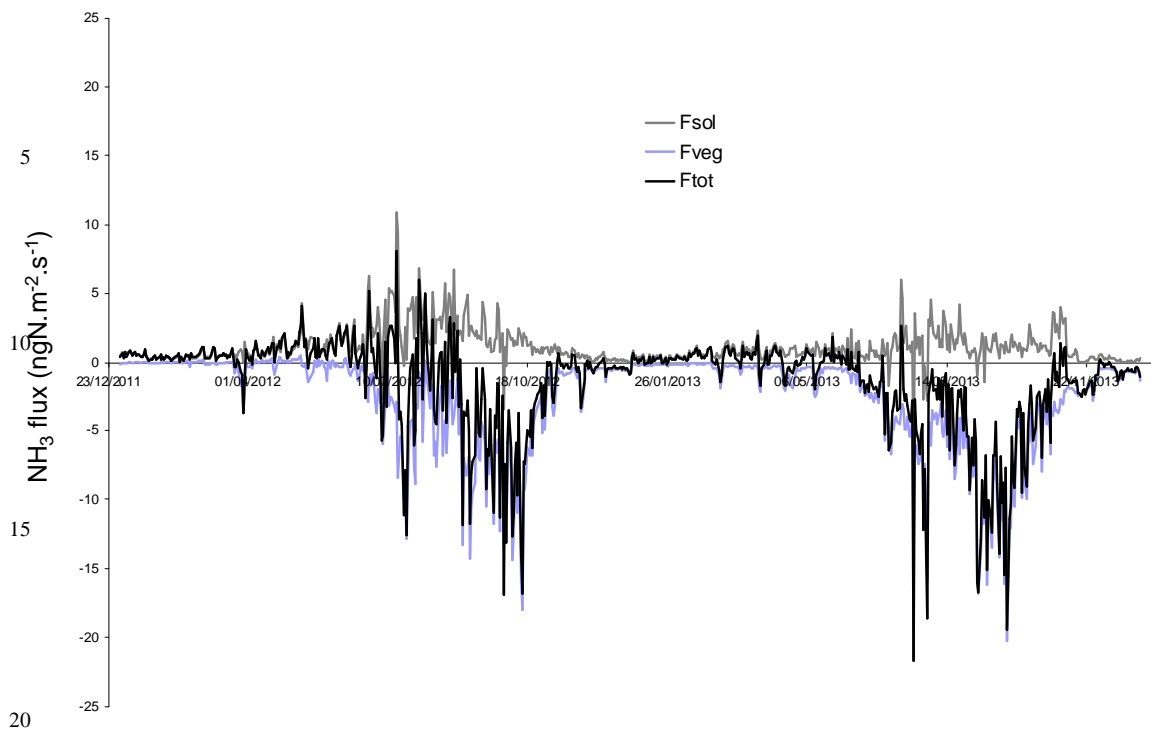
Figure 10: NH$_3$ flux (in ngN.m^{-2}.s^{-1}) simulated by SurfAtm and partitioned between soil and vegetation. Black line is for total net flux (Ftot), grey line is for soil flux (Fsol) and blue line is for vegetation flux (Fveg)